Regional disparities and seasonal differences in climate risk to rice labour

Authors:

1. *Charles Simpson (a) ORCID: 0000-0001-9356-5833
2. J. Scott Hosking (a, c) ORCID: 0000-0002-3646-3504
3. Dann Mitchell (d) ORCID: 0000-0002-0117-3486
4. Richard A. Betts (e,f) ORCID: 0000-0002-4929-0307
5. Emily Shuckburgh (g) ORCID: 0000-0001-9206-3444

Correspondence: charles.simpson@ucl.ac.uk

Affiliations and Addresses:

a) British Antarctic Survey, High Cross, Cambridge, CB3 0ET, United Kingdom
b) Institute for Environmental Design and Engineering, University College London, Central House, 14 Upper Woburn Place, London, WC1H 0NN
c) The Alan Turing Institute, 96 Euston Rd, Somers Town, London NW1 2DB, United Kingdom
d) University of Bristol, University Road, Clifton, Bristol BS8 1SS, United Kingdom
e) Met Office Hadley Centre, FitzRoy Road, Exeter, EX1 3PB
f) University of Exeter Global Systems Institute, Laver Building, North Park Road, Exeter, EX4 4QE, United Kingdom
g) Department of Computer Science and Technology, University of Cambridge, JJ Thomson Ave, Cambridge CB3 0FD, United Kingdom

This document is a preprint submitted to EarthArXiv, it has not been peer reviewed.

This is version 3 of this manuscript. Version 1 was titled Regional disparities in climate risk to rice labour and food security.

Abstract

The 880 million agricultural workers of the world are especially vulnerable to increasing heat stress due to climate change, affecting the health of individuals and decreasing global economic productivity. In this study, we focus on rice harvests across Asia and estimate the future impact on labour productivity by considering changes in climate at the time of the annual harvest. During these specific times of the year, heat stress is often high compared to the rest of the year. Examining climate simulations of the Coupled Model Intercomparison Project 6 (CMIP6), we identified that labour productivity metrics for the rice harvest, based on local wet-bulb globe temperature, are strongly correlated with global mean near-surface air temperature in the long term ($p<<0.01$, $R^2>0.98$ in all models). Limiting global warming to 1.5 °C rather than 2.0 °C prevents a clear reduction in labour capacity of 1% across all Asia and 2% across Southeast Asia, affecting the livelihoods of around 100 million people. Due to differences in mechanization between and within countries, we find that rice labour is especially vulnerable in Indonesia, the Philippines, Bangladesh, and the Indian states of West Bengal and Kerala. Our results highlight the regional disparities and importance in considering seasonal differences in the estimation of the effect of climate change on labour productivity and occupational heat-stress.

1. Introduction

Agricultural workers are especially vulnerable to hot and humid weather, which impacts health and productivity. There are 880 million agricultural workers worldwide (2019 estimate)[1], the majority in low-income countries (LIC) and lower-middle income countries (LMIC). Field studies have demonstrated the presence of heat strain and related health issues in agricultural workers[2–4]. In some places, workers are frequently subject to temperatures in the range considered harmful. Workers self-pace to cope with heat strain, implying a wellbeing trade-off between productivity and thermal comfort. People in the tropics, and outdoor workers especially, will be exposed more frequently to hot and humid conditions in the future due to climate change[5–7].

Ninety percent of global rice production is in Asia, equivalent to 630 million tonnes per year (in 2010-2012)[8,9]. The majority of rice cropland is tropical or subtropical (57% between 23.45 deg N and S, 95% between 35 deg N and S). In the Asia and Pacific region, agriculture employs more than 580 million people (2019 estimate)[1], and rice production comprises 20% of total crop gross production value (2018 estimate)[10]. The labour of rice production is not evenly distributed through the year, and in some locations rice is harvested during the hottest months of the year[4]: this demonstrates that assessments of future impacts on labour productivity should incorporate the seasonality of agricultural labour.

In this article, we estimate the labour productivity effects of climate change for rice harvesting specifically, based on data from global climate models, weather reanalysis, and a database of rice production. Other studies have made estimates of the labour productivity effects of climate change in a more general scope[6,11–13]; we examine some of the assumptions used in these studies. We identify the distribution of labour through the year as an important assumption in relation to agricultural production. We also note the importance of mechanization, the potential for adaptation to higher heat conditions, and the difficulty of accounting for these factors.

2. Methods

The *Methods* section is organised as follows. Subsection 2.1 describes the climate data used in this study, especially global climate model outputs. Subsection 2.2 describes the calculation of heat-stress metrics from the climate data. Subsection 2.3 describes the rice harvest data. Subsection 2.4 explains the statistical experiments and comparisons that were made.

2.1 Climate data

In this study we analyse data from the Coupled Model Intercomparison Project, Phase 6 (CMIP6)[14], comprised of global climate models that have been run in a shared experimental configuration. The model outputs used here are daily mean and maximum temperature, specific humidity, and surface-level air-pressure. All 14 CMIP6 models for which appropriate data were present in the Centre for Environmental Data Analysis (CEDA) archive[1] were included. CMIP historical runs and ScenarioMIP future pathways were processed. ScenarioMIP runs simulate the future climate given assumptions about future emissions (especially of greenhouse gases) and development pathways called Shared Socioeconomic Pathways (SSPs)[15]. So that models with multiple ensemble members were not given additional statistical weight, a single ensemble member was used for each model, selected in numerical order from what was available in the archive. A table of model runs used, with data citations, is included in the supplementary material (Supplementary tables 2 and 3). Although SSPs contain socioeconomic assumptions, we did not make any direct use of the socioeconomic data associated with each SSP; we used only atmospheric variables.

The Climatic Research Unit gridded Time Series (CRUTS) 4.03[16,17], and the European Centre for Medium-Range Weather Forecasts Reanalysis 5 (ERA5)[18], were used as historical observational datasets.

Daily frequency CMIP6 data were used. Sub-daily data for the variables of interest were available for only a small number of models. Daytime temperature variation was estimated by assuming the temperature is close to the daily mean temperature, daily max temperature, and the mid-point of the two, for 4 hours each, following Kjellstrom et al (2018)[6]. Comparing the result of this calculation using 3-hourly and daily

[1] http://archive.ceda.ac.uk/

CMIP6 data, we found that this is a reasonable approximation. Daily ERA5 data were used to maintain consistency with the CMIP6 data. CRUTS 4.03 is monthly and is only included as a crosscheck.

2.2 Heat stress calculations

Wet-bulb globe temperature (WBGT) is a heat-stress metric defined by ISO 7243 and widely used for assessing hazards due to hot conditions[19–21] . WBGT is intended to combine the factors that affect the human experience of heat: namely air temperature, radiant temperature, humidity, and air velocity[20]. WBGT is designed to be measured directly using specialised equipment; in practice, statistical and empirical formulae for estimating it from standard meteorological variables must be used in the climate context. We assumed that work occurs in the shade, so that air temperature approximates black-globe temperature (BGT). Furthermore, cloud cover is one of the most uncertain aspects of global climate models[22]. In the supplementary material (supplementary section 2.1), we explore the effect of excluding radiation. Although this leads to underestimation of heat stress in some conditions, we find that long-term trends in WBGT are determined mainly by changes in air temperature. Furthermore, this assumption is used in other related studies[6,11,12].

WBGT was calculated as $\mathrm{WBGT} = 0.7 * \mathrm{WBT} + 0.3 * \mathrm{BGT}$, where WBT is the wet-bulb temperature. WBT was calculated from air temperature, specific humidity, and air pressure using open-source software 'psychrolib'[23] which implements formulae from the American Society of Heating, Refrigerating and Air-Conditioning Engineers handbook. Field measured WBT decreases with wind speed at low speed (<2 m/s, a light breeze), but higher wind speeds have a lesser effect[24]. The WBT calculation used is consistent with a light breeze, and variation in wind speed is neglected.

Studies of occupational heat stress under climate change often either assume a threshold in WBGT above which a worker is at risk[25], or assume that there is a simple relationship between WBGT and worker productivity. Typically, these relationships are assumed to be representative across sectors, and are based on either a regulatory or advisory standard[11], limited field study or survey data, or an ad hoc fusion of the two[6,12,26]. Occupational heat-stress regulations attempt to minimise harm and are often exceeded in

practice. Therefore, use of regulatory standards to estimate future labour-productivity, as in Dunne et al. (2013)[11], may not be accurate. Field data measuring the effect of heat on worker productivity are sparse and cover only a few activities. Studies of small numbers of workers are often used to estimate productivity effects on the entire human population.

Sahu et al (2013)[4] observed a 5% per °C WBGT decrease in the labour capacity of labourers harvesting rice between 26-32 °C WBGT. Rate of collection was measured in 124 workers in groups of 10-18, and WBGT was measured in-situ, at an individual location in India. For our study, we assume that this is representative of manual rice harvest labour, and adopt it as our labour impact metric. By labour impact metric, we mean the amount that labour productivity is reduced by heat stress. The impact is assumed to be linear in WBGT, although this assumption must break down at high WBGT (>35 °C). The systematic uncertainty due to these assumptions cannot be assessed without larger scale field observations. The labour impact metric is calculated as $5.14 * \mathrm{WBGT} - 218$, in units of %, clipped at 0 and 100, meaning that 0% loss occurs at 23 °C and 100% loss occurs at 42.5 °C. This function comes from interpretation of the Sahu et al. (2013) study by Gosling et al. (2018). By using a labour impact derived from a study specific to manual rice harvesting, we represent this particular activity more accurately than the assumptions used for the economy in general in other studies (e.g. [6,11,12,25–27]).

To facilitate comparison to other studies, results were also calculated using different assumptions about the relationship between WBGT and labour productivity: the assumptions used for agricultural labour in Dunne et al. (2013)[11], and in Orlov et al. (2020)[27]. Our calculations are consistent with these other studies above. In the supplementary material (Supplementary Section 2.2), equations for each of these and the effect of varying the assumptions are shown.

2.3 Rice data

The RiceAtlas dataset[8,9] provides detailed data on rice production, broken down into location entities with an average area of 5000 km^2. Information such as yield, harvested area, planting and harvesting dates are included, and many entities have multiple yearly harvests. The data are representative of the years

2010-2012. We used this to identify harvest dates. Location entities in RiceAtlas vary greatly in size, and many are much smaller than the grid spacing of the climate models considered. Where a location geometry enclosed multiple climate-model grid-cells, the mean was taken of the enclosed cells; otherwise, the land grid-point closest to the centroid of the location was used. We used data only for countries in Asia; see Table 1. The distribution of rice cropland in Asia is shown in Figure 1.

2.4 Statistical experiments and comparisons

For each location and harvest season, climate data (ERA5 and CRUTS 4.03, and CMIP6 outputs) were selected using the harvest dates and spatial geometry provided by RiceAtlas, and WBGT calculated. Only climate data during the peak month of each harvest were selected. Then, the labour impact metric was calculated from WBGT. Independently for each climate model, and for each location and season, a linear trend was fitted between the 20-year means of the change in the global mean near-surface air temperature (GSAT) and the labour productivity metric. Twenty-year periods were defined between 1850-2009 inclusive for the historical runs, 2020-2099 inclusive for the SSP runs. As the labour productivity function was clipped at zero, the fitted function was too. We assumed that 1 °C of GSAT warming relative to 1850-1900 was representative of the present (2020)[28], and changes in both variables are relative to the present. Data from historical model runs and different SSPs were included together in a single fit, so that a range of GSAT values (up to 4 °C relative to 1850-1900) were included; but each model, and harvest season and location was fit independently. We defined the gradient of this fit as the “hazard gradient”, the purpose of which is to summarise the relationship between changes in GSAT and local changes in labour productivity via WBGT, to explore the spatial patterns of change. The hazard gradient means the amount by which the labour impact increases on average for 1 °C of global warming. This effectively collapses variation in time, the climate sensitivity of each model, and emissions scenario into a single dimension. The two-sided inverse student’s t-distribution was used to determine whether the hazard gradient in each harvest season and location was significant.

The multi-model mean of the hazard gradient was calculated for each harvest season and location. The labour impact was also averaged over all locations, weighted by total rice production, to characterise the regional situation.

Statistical tests were applied to the results. In order to test if there was a significant change in the historical period, linear regression was used on the time-series of the labour impact metric calculated from ERA5 and CRU-TS, and the two-sided inverse student's t-distribution used to determine if the gradient was significantly different from zero. To test if there is a significant difference between different warming scenarios, the distributions of results across climate models at 1.5, 2.0, and 3.0 °C of global warming were compared using the Kolmogorov-Smirnov (KS) test and student's T test.

3. Results

3.1 Regional Results

Figure 2 shows the Asia-wide average of the heat impact on rice harvest labour, calculated from the historical observational and reanalysis datasets, weighted by total rice production in each harvest season and location. There is a statistically significant increase ($p<<0.01$) over the full observational period (1900-2018) of CRU-TS, and in both datasets for the common observational period (1980-2018): the heat hazard associated with the rice harvest has already increased.

Figure 3 shows heat impact on Asia-wide rice harvest labour plotted against GSAT warming across various climate models. Changes are relative to the present, assumed to mean 1 °C of warming over 1850-1900. The rice harvest labour impact is weighted by total rice production. In Figure 3a, each point is a 20 year mean in a single model simulation. Despite the different biases and climate sensitivities of the models, they each show a linear relationship between GSAT and the rice harvest labour impact. All models have a hazard gradient 2.0-2.7 %/°C, $p<<0.01$, $R^2>0.98$. The multi-model mean (standard deviation) of the hazard gradient is 2.3 (0.2) %/°C. A single trend line is shown in figure 3a for illustration only.

In Figure 3b, the Asia-wide labour impact is linearly interpolated to 1.5, 2.0 and 3.0 °C of warming (relative to 1850-1900) individually for each model, and results are shown as a multi-model boxplot. There is

a statistically significant difference between the 1.0 °C and 1.5 °C of warming with multi-model mean (standard deviation) 1.0 (0.3) %; between 1.5 and 2.0 °C of 1.3 (0.2) %; as well as between 2.0 and 3.0 °C of 2.6 (0.4) %. KS test and T test p-values on the multi-model distributions are small (<<0.001) for each case.

As the Asia-wide analysis is weighted according to total rice production in each location and season, the Asia-wide results should be interpreted carefully: the average is more sensitive to locations with more intensive cropping. However, the breakdown by location shows that the trends are general, and not skewed by a single area with high cropping intensity. The correlation coefficient of the hazard-gradient between models and within each harvest season and location is 0.95, suggesting that there is generally high agreement between the models.

3.2 Local and seasonal results

Figure 4 shows the distribution of the multi-model mean hazard-gradient across harvest seasons and locations. In the blue histogram, the entire year is given equal weight in the heat stress calculation. Conversely, in the orange histogram, only the rice harvest season is considered in the heat stress calculation. Both histograms are weighted by rice production. Considering the time of year at which the rice harvest occurs, as opposed to the whole of the year, leads to some rice harvests having higher hazard-gradient, but other harvests not having a significant hazard-gradient. If the harvest season and locations with non-significant hazard-gradients are excluded, then the mean hazard-gradient is increased. The interquartile range of the distribution in orange is more than double that in blue. The two assumptions lead to completely different distributions of hazard gradient, showing the importance of including the seasonality of labour in projections of the effect of heat-stress on agricultural labour productivity.

The 50% of rice production with the highest hazard gradients (hazard gradient >3.05 %/°C) is identified as being exposed to a high hazard-gradient; the proportion of exposed production in each location is mapped in Figure 5 and listed by country in Table 1. We do this to identify regional differences in the estimated labour impact; we are not suggesting this is a limit to adaptation. Areas identified by this method

include most of Southeast Asia, and coastal South Asia. Harvests in northern India (e.g., in Punjab) are not strongly affected.

Figure 6 shows the hazard gradient for each harvest season and location, plotted against latitude in 6a and against the peak month of the harvest season in 6c. Figure 6b shows the hazard gradient against latitude assuming the full year is equally weighted. Two interacting effects explain most of the spatial variation in the results. Firstly, locations close to the equator have higher temperatures. Secondly, for locations that are further from the equator there is greater seasonal variation in temperature, so the time of year at which the harvest occurs is important. Figure 6b shows that if the time of year of the harvest is not considered, then the hazard gradient is mostly determined by latitude. As Figure 6c shows, all large harvests that are not exposed to high hazard-gradients peak between September and December inclusive. Close to the equator, for example in Indonesia, hazard gradient is not very seasonally dependent as there is little seasonal variation in temperature. By comparison, in China and India the time of year of the harvest season has a much stronger effect on the hazard gradient.

4. Discussion

4.1 Large scale trends

Global mean surface temperature (GMST) has increased by 0.9-1.2 °C relative to 1850-1900 as of 2017[28], and if anthropogenic warming continues to follow recent trends, is projected to reach 1.5 °C between 2030 and 2052; the estimated rate of warming is 0.2 °C per decade[29]. In accordance with the Paris Agreement under the United Nations Framework Convention on Climate Change[30], most countries have committed to limit GMST warming by 2100 to 2 °C, and to make efforts to limit warming to 1.5 °C. However, at the time of writing, pledges of emissions reductions are not sufficient to meet this goal[31].

We identify in Figure 2 that there is a statistically significant increase in the estimated heat impact in the historical observational dataset. However, we do not know of any comparable data that attempts to directly measure the heat strain that farm workers are under on a regional or global scale, so the full effects of this are unclear.

Overall, the long-term averages in the estimated labour impact are highly correlated with GSAT change (Figure 3). This is not surprising as the labour impact metric is linear in WBGT above a threshold, and GSAT change (i.e., global warming) dominates large-scale, long-term trends in WBGT. This relationship holds at the Asia-wide level, but also individually for most location and seasons.

4.2 Seasonality

Labour inputs to rice production are seasonal, with more labour occurring around planting and harvesting[32–3]>. This labour cannot be delayed or displaced to other times of year, and the timeliness of these activities affects yield and quality. Averaging across the full year assumes that labour for any given activity can be exchanged with labour at a different time of year, which is clearly not the case for planting and harvesting. In this study, we have shown the importance of considering the seasonality of agricultural labour when estimating the effect of heat-stress on labour productivity. We have focussed only on harvesting, and only on rice. However, most crops are seasonal, and therefore have a seasonal distribution of labour; this should be taken into account in estimates of the effect of heat stress on labour. Other studies into the effect of climate change on labour productivity, even those focussed on agricultural labour, do not take this into account[6,12,13,27].

In some cases, for example wheat in Punjab, rice is multi-cropped with another crop that is not covered in this study, but for which harvest labour may be more exposed. Studies have suggested that changes to planting and harvesting dates[3]>, and crop choice[36], could be used to adapt to climate change and mitigate negative effects on yields. Changes to planting and harvesting dates, to maximise yield as temperature and precipitation patterns change, is a complex topic, and outside the scope of this study. Given that the world has already experienced 1 °C of warming, such adaptations may already be occurring. Changes to planting and harvesting dates could lead to workers being exposed to heat stress in locations where they currently are not, and this should be considered when studying adaptive measures.

4.3 Mechanisation

Farm mechanisation in Asia over the past 50 years has been driven by small internal combustion engines, which have already alleviated much of the human drudgery of farming, reduced the use of draft animals, and increased yields[37,3]>. However, more fatal injuries occur when using powered machinery[38], and the use of internal combustion engines contributes to greenhouse gas emissions. High-quality international data on farm mechanization are lacking. Differences in mechanisation between LIC is not a simple function of gross domestic product. Mechanization of power intensive operations such as pumping, tilling, and threshing often coexist with manual seeding, weeding, crop care, and harvesting. Mechanization of power intensive operations is economically advantageous, even when wages are low, if demand for crops favours intensification. Remaining manual operations tend to be mechanized when agricultural wages rise due to economic development[39]. Power intensive operations are widely mechanized across Asia[37,39,40], and manual operations may gradually disappear because of economic development. Vulnerability may be higher in parts of sub-Saharan Africa, or for other crops, where there has been less uptake of agricultural machinery[39,40].

A survey of farms close to research centres by Bordey et al. (2016)[3]> suggested that production is much more labour intensive in the Philippines, Indonesia, and India, (>65 worker-days per hectare) compared in China, Thailand, and Vietnam (10-20 worker-days per hectare). The rice bowl regions of Thailand and the Philippines have high levels of mechanization for land preparation, but animal draft power is still used in more agriculturally marginal areas[39]. Mechanization in India varies between states. Four-wheel tractor (4WT) density is highest in Haryana[2] and Punjab (>100 4WT per 1000 ha), and lowest in Kerala and West Bengal (<10 4WT per 1000 ha)[40] (2012 estimates). Assuming mechanization is homogeneous across a large country such as India will lead to underestimating the vulnerability of some locations. In Bangladesh, land preparation is mechanized, but harvesting is not[40,41], with on average 5 4WTs per 1000 ha and 0.01 combine harvesters per 1000 ha (2014 estimates). Other locations are exposed to the hazard, and may be vulnerable, but data concerning mechanization of harvests is lacking.

[2] Subnational locations mentioned in the article have Hierarchical administrative subdivision codes (HASC) listed in supplementary table 1. A full list of HASC with country, region, and sub-region names is included in the data supplement.

4.4 Limitations

Workers may be able to reduce heat exposure by starting work early in the morning when it is cooler, but this could mean working in the dark. Reducing work hours could also reduce heat exposure but could exacerbate labour shortage. We note that the workers observed by Sahu et al (2013) began their work near dawn and were still exposed to hazardous heat in their first hour of work[4].

The accuracy, coverage, and granularity of the rice crop data limits our study. However, by focussing on long-term trends with high levels of multi-model agreement, we avoid the issue of climate model bias. The assumed linear effect of WBGT on labour productivity comes from a single field study and cannot be accurate as WBGT approaches known human physiological limits, but the general conclusions are unchanged by substituting other labour-impact functions from the literature (see Supplementary Section 2.2). Due to the resolution of climate models, results will be less reliable for locations with steep gradients in altitude, for example Nepal.

El Nino is an important driver of annual temperature variation in the region, and negatively affects crops through rainfall patterns (see e.g. Selvaraju (2003)[4]>). Higher global temperatures could change El Nino patterns, but this is beyond the scope of this study. We have focussed on long term trends on the scale of 20 years rather than extreme events, but WBT extremes are also closely correlated with large-scale mean temperatures within the tropics[43].

5. Conclusion

The rising impact of heat on rice harvest labour will be unevenly distributed, falling on poor rural workers who will be least able to adapt, and therefore contributing to widening economic inequality. Given agriculture employs hundreds of millions of people, a few-percent shift in labour capacity is equivalent to the labour of millions of people. Labour productivity decreases due to climate change will compound other environmental impacts on rice production, including declining yields as direct result of increasing

temperature[4]>, water stress, and sea level rise[29]; contributing to the unequal loss and damage created by climate change.

We see a strong relationship between heat hazard and GSAT change in the rice harvest seasons and locations of Asia, with a high level of agreement between climate models. Historical observational data already shows a statistically significant increase in our labour impact metric. Understanding disparities in the heat-stress exposure of workers and industries around the world will be important for climate adaptation strategy, as well as estimation of loss and damage. Overall, the exposure of such a large proportion of rice agriculture, and the workers engaged therein, provides an argument for strong mitigation of climate change.

We have chosen to focus on rice harvesting, but all of issues discussed apply to other crops: key activities have different amenability to mechanization and different work intensities, and labour is not evenly spread throughout the year. Assuming that labour is equally distributed through the year leads to underestimation of the effect of climate change on the heat stress of agricultural workers in many places. Accurate accounting for the balance of mechanization and manual labour remains difficult.

Figures and Tables

Table 1: Rice production exposed to hazard gradient above the 50th percentile by country, and Asia total. Countries with less than 1 million tonnes of annual rice production are not included. Rice production from RiceAtlas[8]. We define hazard gradient as the gradient between GSAT and local labour impact.

COUNTRY	Production above 50th percentile of hazard gradient (%)	Total production (million tonnes)	Production above 50th percentile of hazard gradient (million tonnes)
Asia	50	646	323
Indonesia	100	67	67
India	36	151	55
China	27	200	55
Vietnam	83	42	35
Thailand	77	36	28
Bangladesh	61	45	27
Myanmar	71	32	23
Philippines	94	17	16
Cambodia	75	9	7
Sri Lanka	100	4	4
Malaysia	100	3	3
Japan	29	8	2
Taiwan	70	2	1
Laos	25	3	1
South Korea	0	6	0
Nepal	0	5	0
North Korea	0	2	0
Pakistan	0	9	0
Iran	0	3	0

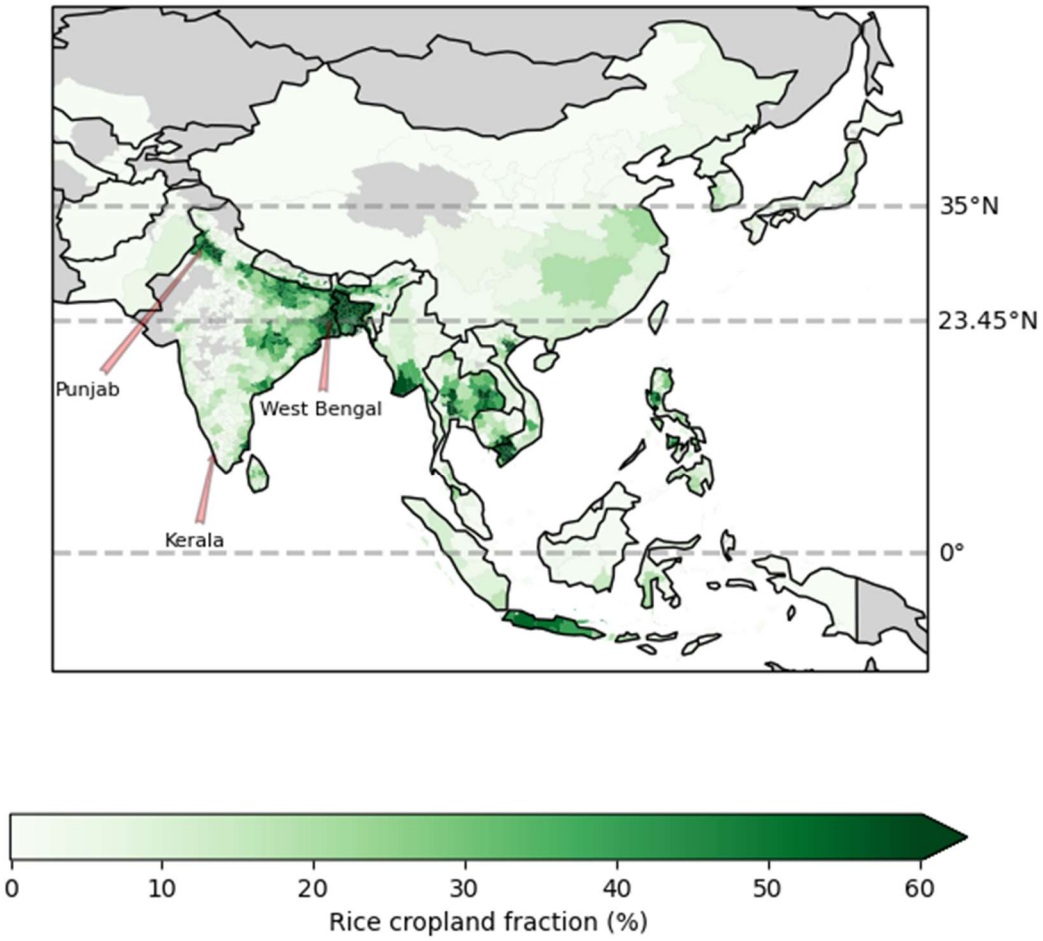

Figure 1: Geographical distribution of rice production across Asia (green shading). Sub-national locations mentioned in the article are labelled. Data sourced from RiceAtlas[8].

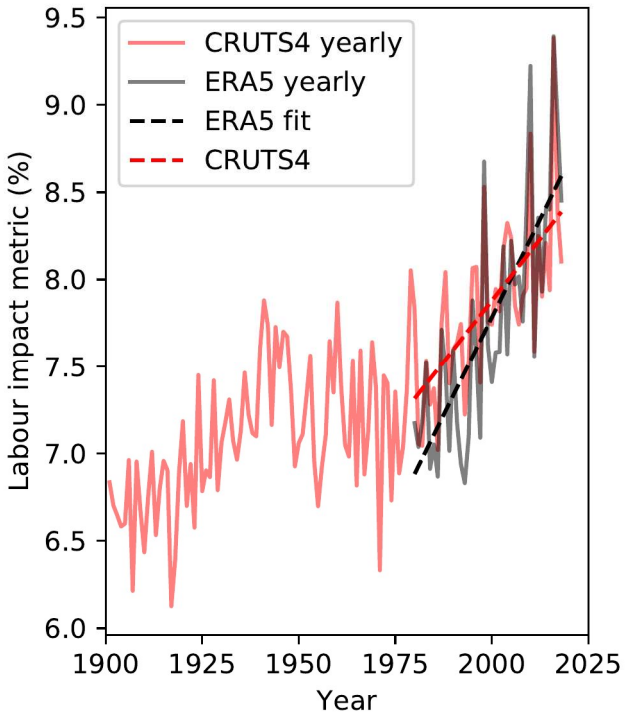

Figure 2: Annual Asia-wide mean labour impact, weighted by total rice production, calculated from CRU-TS 4.03 (red lines) and ERA5 (black line), with trend lines (dashed) shown for the period 1980-2018.

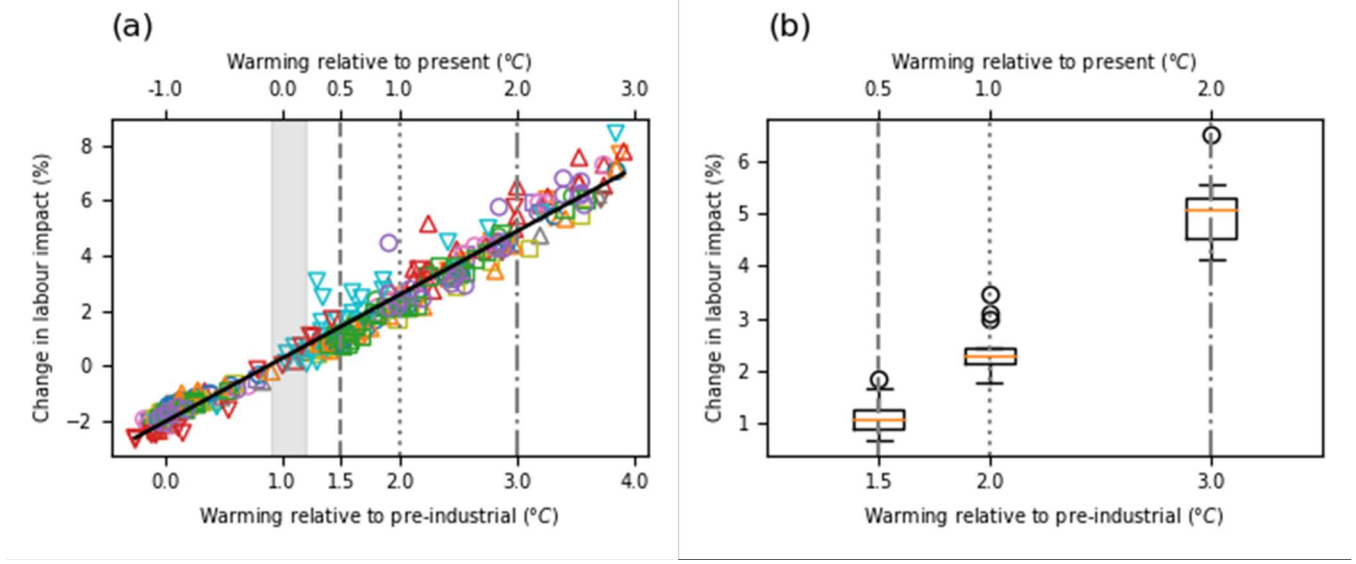

Figure 3: Relationship between rice labour impact and GSAT change in the 14 analysed CMIP6 climate models; Changes are relative to 1.0 C of warming relative to 1850-1900, which is assumed to represent the present. Three levels of warming relative to 1850-1900 and relative to the present are shown for context. The present estimated range of warming is shown by the grey shading. (a) Change in labour impacts against GSAT for 20 year periods; each shape/colour corresponds to a different model The black trend line is illustrative only: fit statistics mentioned in the text are based on fitting each climate model individually. (b) Change in labour impacts at three levels of warming, with box plot to show climate model spread. Points are linearly interpolated to the three levels of warming. Boxes show 1st (Q1) and 3rd quartile (Q3); orange line at the median; lower whiskers at lowest point above Q1–1.5(Q3-Q1), upper whiskers highest point below Q1+1.5*(Q3-Q1); circles are points outside the whisker range. We define hazard gradient as the gradient between GSAT and local labour impact.*

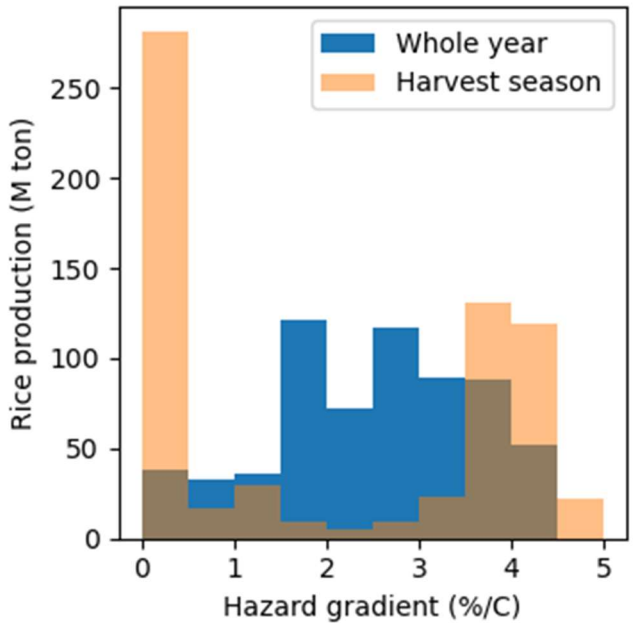

Figure 4: Histograms showing the distribution of hazard gradient across harvest seasons and locations. The effect of seasonal weighting assumptions on the hazard gradient is shown: the blue histogram represents the assumption that the whole year is equally weighted, while the orange histogram shows the result if only the rice harvest season is included. The histograms are weighted by the harvest weight in millions of tonnes.

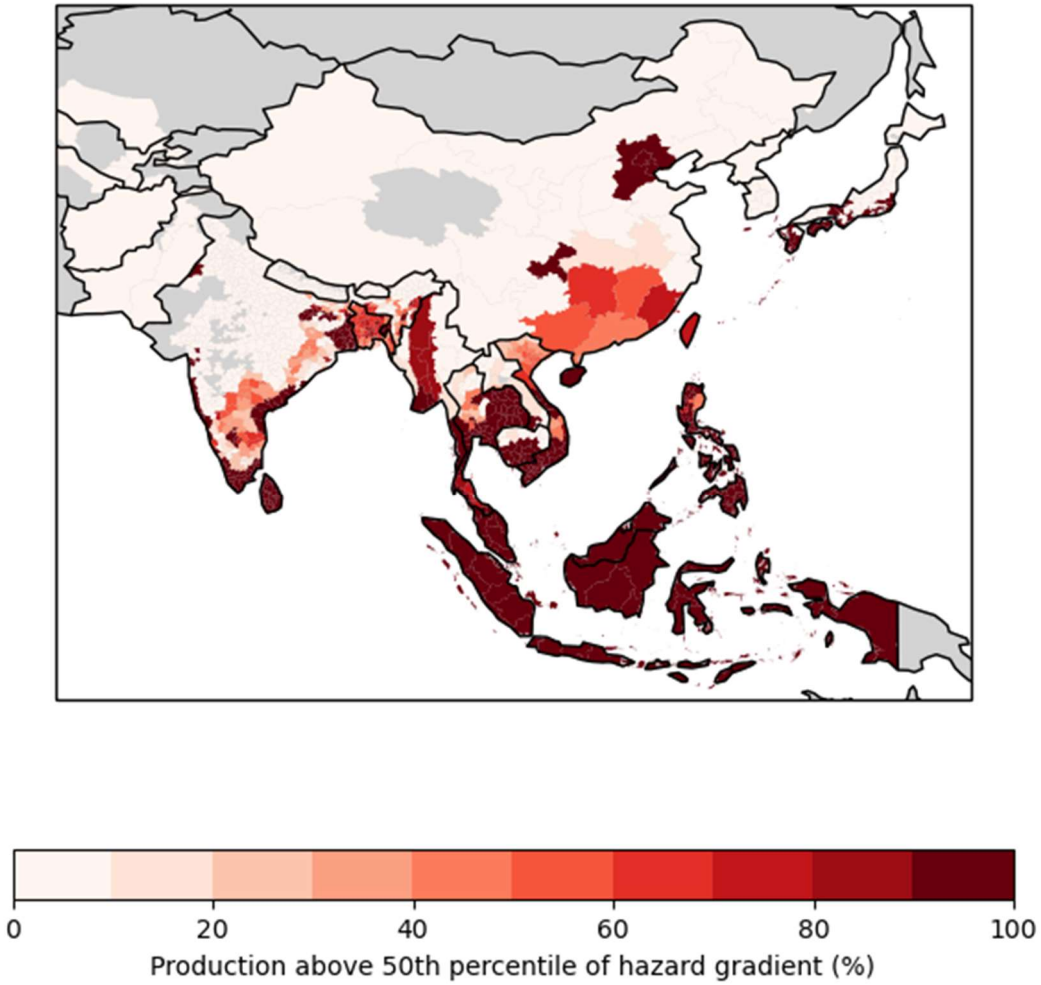

Figure 5: Map of Asia with shading representing proportion of rice production in harvests for which labour capacity is identified as being in the higher 50% of hazard-gradient.

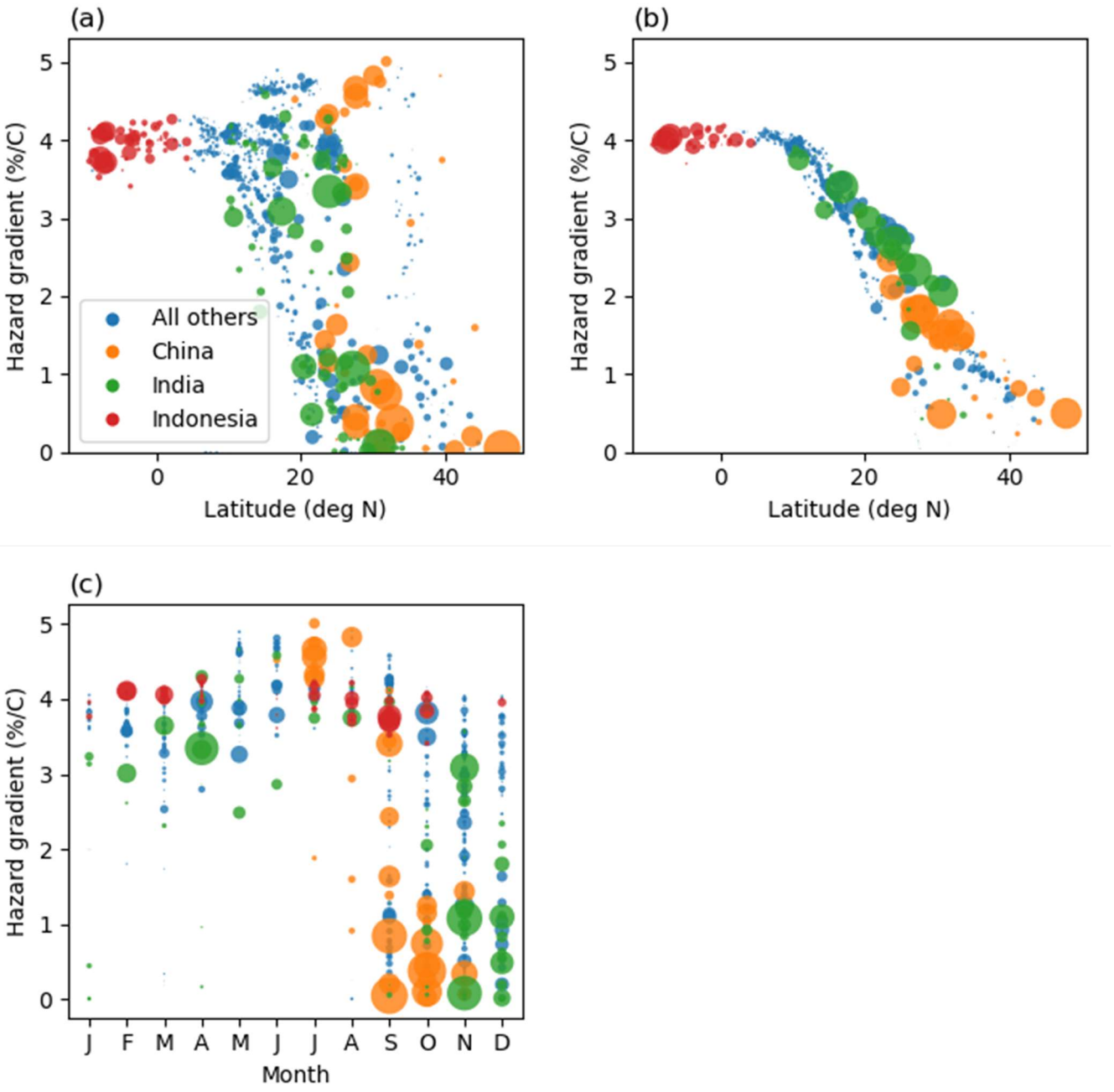

Figure 6: Scatter plots, with marker size proportional to total harvest weight, of hazard gradient for each location and season: (a) plotted against latitude, selecting only the peak of the rice harvest; (b) plotted against latitude, averaged over the whole year equally; (c) plotted against peak month of harvest. Colours identify points belonging to China, India, and Indonesia. Hazard gradients are multi-model means. In order to reduce the number of markers, some aggregation was performed: in both cases the mean weighted by total weight of harvested rice was taken; the results were aggregated to the 2nd level HASC geocode, independently for each month.

Acknowledgements

All authors are funded by the NERC EMERGENCE project: CS, JSH and ES by NE/S004726/1, RAB by NE/S004645/1, and DM by NE/S005242/1. The work of RAB also forms part of the BEIS/Defra Met Office Hadley Centre Climate Programme (GA01101). CS is also funded by the Wellcome HEROIC project. This project made use of the JASMIN computer service (jasmin.ac.uk), and CEDA archive (ceda.ac.uk). Thanks to the developers of the following software packages: Geopandas, Xarray, Cartopy, Psychrolib. We acknowledge the World Climate Research Programme, which, through its Working Group on Coupled Modelling, coordinated and promoted CMIP6. We thank the climate modelling groups for producing and making available their model output, the Earth System Grid Federation (ESGF) for archiving the data and providing access, and the multiple funding agencies who support CMIP6 and ESGF.

Data and code availability statement

The datasets generated during the study are freely available from Zenodo https://doi.org/10.5281/zenodo.4737471. A code demonstration can be found at https://doi.org/10.5281/zenodo.4746392.

Author contribution statement

CS performed the analysis and mostly wrote the paper. JSH, DM, RAB, and ES helped develop the ideas for the analysis, and advised on the wording and emphasis of the paper.

Competing interest statement

The authors declare no competing interests.

References

1. International Labour Organization. Employment by sex and economic activity -- ILO modelled estimates. https://ilostat.ilo.org/ (2019).

2. Moyce, S. *et al.* Heat strain, volume depletion and kidney function in California agricultural workers. *Occup. Environ. Med.* **74**, 402–409 (2017).

3. Crowe, J. *et al.* Heat exposure in sugarcane harvesters in Costa Rica. *Am. J. Ind. Med.* **56**, 1157–1164 (2013).

4. Sahu, S., Sett, M. & Kjellstrom, T. Heat Exposure, Cardiovascular Stress and Work Productivity in Rice Harvesters in India: Implications for a Climate Change Future. *Ind. Health* **51**, 424–431 (2013).

5. Zhao, Y., Ducharne, A., Sultan, B., Braconnot, P. & Vautard, R. Estimating heat stress from climate-based indicators: Present-day biases and future spreads in the CMIP5 global climate model ensemble. *Environ. Res. Lett.* **10**, 84013 (2015).

6. Kjellstrom, T., Freyberg, C., Lemke, B., Otto, M. & Briggs, D. Estimating population heat exposure and impacts on working people in conjunction with climate change. *Int. J. Biometeorol.* **62**, 291–306 (2018).

7. Coffel, E. D., Horton, R. M. & De Sherbinin, A. Temperature and humidity based projections of a rapid rise in global heat stress exposure during the 21st century. *Environmental Research Letters* vol. 13 (2018).

8. Laborte, A. G. *et al.* RiceAtlas, a spatial database of global rice calendars and production. *Sci. Data* **4**, 1–10 (2017).

9. Laborte, A. G. *et al.* RiceAtlas, a spatial database of global rice calendars and production (dataset). (2017) doi:10.7910/DVN/JE6R2R.

10. Food and Agriculture Organization of the United Nations (FAO). Value of Agricultural Production. *License: CC BY-NC-SA 3.0 IGO* http://www.fao.org/faostat/en/#data/QV/ (2019).

11. Dunne, J. P., Stouffer, R. J. & John, J. G. Reductions in labour capacity from heat stress under climate warming. *Nat. Clim. Chang.* **3**, 563–566 (2013).

12. Watts, N. *et al.* The 2020 report of The Lancet Countdown on health and climate change: responding to converging crises. *The Lancet* vol. 397 129–170 (2021).

13. De Lima, C. Z. *et al.* Heat stress on agricultural workers exacerbates crop impacts of climate change. *Environ. Res. Lett* **16**, 44020 (2021).

14. Eyring, V. *et al.* Overview of the Coupled Model Intercomparison Project Phase 6 (CMIP6) experimental design and organization. *Geosci. Model Dev* **9**, 1937–1958 (2016).

15. O'Neill, B. C. *et al.* The Scenario Model Intercomparison Project (ScenarioMIP) for CMIP6. *Geosci. Model Dev.* **9**, 3461–3482 (2016).

16. Harris, I., Osborn, T. J., Jones, P. & Lister, D. Version 4 of the CRU TS monthly high-resolution gridded multivariate climate dataset. *Sci. Data* **7**, 1–18 (2020).

17. University of East Anglia Climatic Research Unit, Harris, I. C. & Jones, P. D. CRU TS4.03: Climatic Research Unit (CRU) Time-Series (TS) version 4.03 of high-resolution gridded data of month-by-month variation in climate (Jan. 1901- Dec. 2018). (2020) doi:10.5285/10d3e3640f004c578403419aac167d82.

18. Hersbach, H. *et al.* The ERA5 global reanalysis. *Q. J. R. Meteorol. Soc.* **146**, 1999–2049 (2020).

19. Epstein, Y. & Moran, D. S. Thermal Comfort and the Heat Stress Indices. *Ind. Health* **44**, 388–398 (2006).

20. Parsons, K. Heat stress standard ISO 7243 and its global application. *Industrial Health* vol. 44 368–379 (2006).

21. Parsons, K. Occupational Health Impacts of Climate Change: Current and Future ISO Standards for the Assessment of Heat Stress. *Ind. Health* **51**, 86–100 (2013).

22. Vial, J., Dufresne, J.-L. & Bony, S. On the interpretation of inter-model spread in CMIP5 climate sensitivity estimates. *Clim. Dyn.* **41**, 3339–3362 (2013).

23. Meyer, D. & Thevenard, D. PsychroLib: a library of psychrometric functions to calculate thermodynamic properties of air. *J. Open Source Softw.* **4**, 1137 (2019).

24. Lemke, B. & Kjellstrom, T. Calculating Workplace WBGT from Meteorological Data: A Tool for Climate Change Assessment. *Ind. Health* **50**, 267–278 (2012).

25. Andrews, O., Le Quéré, C., Kjellstrom, T., Lemke, B. & Haines, A. Implications for workability and survivability in populations exposed to extreme heat under climate change: a modelling study. *Lancet Planet. Heal.* **2**, e540–e547 (2018).

26. Gosling, S. N., Zaherpour, J. & Ibarreta, D. *PESETA III: Climate change impacts on labour productivity*. (Publications Office of the European Union, 2018). doi:10.2760/07911.

27. Orlov, A., Sillmann, J., Aunan, K., Kjellstrom, T. & Aaheim, A. Economic costs of heat-induced reductions in worker productivity due to global warming. *Glob. Environ. Chang.* **63**, (2020).

28. Haustein, K. *et al.* A real-time Global Warming Index. *Sci. Rep.* **7**, 1–6 (2017).

29. Masson-Delmotte, V. *et al. Global warming of 1.5°C*. (International Panel on Climate Change, 2019).

30. Conference of the Parties. *Adoption of the Paris Agreement*. U.N. Doc. FCCC/CP/2015/L.9/Rev/1 (2015).

31. Raftery, A. E., Zimmer, A., Frierson, D. M. W., Startz, R. & Liu, P. Less than 2 °c warming by 2100 unlikely. *Nat. Clim. Chang.* **7**, 637–641 (2017).

32. Singh, G. & Chancellor, W. Energy Inputs and Agricultural Production under Various Regimes of Mechanization in Northern India. (2016) doi:10.13031/2013.38695.

33. Bordey, F. H., Moya, P. F., Beltran, J. C. & Dawe, D. C. *Competitiveness of Philippine Rice in Asia*. *International Rice Research Institute* (Philippine Rice Research Institute, 2016).

34. Quilty, J. R. *et al.* Energy efficiency of rice production in farmers' fields and intensively cropped research fields in the Philippines. *F. Crop. Res.* **168**, 8–18 (2014).

35. Jalota, S. K. *et al.* Mitigating future climate change effects by shifting planting dates of crops in rice-wheat cropping system. *Reg. Environ. Chang.* (2012) doi:10.1007/s10113-012-0300-y.

36. Kurukulasuriya, P. & Mendelsohn, R. *Crop switching as a strategy for adapting to climate change*. *African Journal of Agricultural and Resource Economics* vol. 2 http://ageconsearch.umn.edu/record/56970 (2008).

37. Justice, S. & Biggs, S. The spread of smaller engines and markets in machinery services in rural areas of South Asia. *J. Rural Stud.* **73**, 10–20 (2020).

38. Nag, P. K. & Nag, A. Drudgery, Accidents and Injuries in Indian Agriculture. *Industrial Health* vol. 42 149–162 (2004).

39. Pingali, P. Agricultural Mechanization: Adoption Patterns and Economic Impact. in *Handbook of Agricultural Economics* vol. 3 2779–2805 (Elsevier, 2007).

40. Diao, X., Takeshima, H. & Zhang, X. *An evolving paradigm of agricultural mechanization development: How much can Africa learn from Asia?* (International Food Policy Research Institute (IFPRI), 2020). doi:10.2499/9780896293809.

41. Islam, A. K. M. S. Status of rice farming mechanization in Bangladesh. *J. Biosci. Agric. Res.* **17**, 1386–1395 (2018).

42. Selvaraju, R. Impact of El Niño-southern oscillation on Indian foodgrain production. *Int. J. Climatol.* **23**, 187–206 (2003).

43. Zhang, Y., Held, I. & Fueglistaler, S. Projections of tropical heat stress constrained by atmospheric dynamics. *Nat. Geosci.* **14**, 133–137 (2021).

44. Welch, J. R. *et al.* Rice yields in tropical/subtropical Asia exhibit large but opposing sensitivities to minimum and maximum temperatures. *Natl. Acad Sci.* **107**, 14562–14567 (2010).

Supplementary Material

1. Rice production statistics

The majority of rice production in Asia is tropical or sub-tropical, as can be seen in the Supplementary Figure 1. As shown in Supplementary Figure 2, harvesting occurs throughout the year, but with more occurring in September-November. For a more complete illustration of the timing of harvest seasons in the RiceAtlas dataset, we refer to the paper describing that dataset[1].

2.1 Evaluation of assumptions

Key assumptions in this work are: (1) the parameterisation of the daily variation, (2) neglect of radiation, and (3) the labour impact metrics. In order to demonstrate the robustness of our results, we repeated the analysis with 3-hourly CMIP6 data (henceforth '3hd'), for a single models and single SSP scenario. The overall conclusions of the analysis (that the metric is strongly correlated with global mean surface temperatures, and that it is important to incorporate the seasonal variation of labour into assessments) are robust against these changes of assumption.

The model used with 3hd was HadGEM3-GC31-LL. This is not the same as the set of models used in the main analysis. Availability of data via the CEDA archive determined the selection. To simplify the 3hd calculation, the labour impact metric was aggregated to a monthly time basis, and harvest seasons selected by peak month, rather than using the day of the year. SSP 245 was used.

In the main analysis of this study we assumed that the temperature is close to the daily mean temperature, daily max temperature, and the mid-point of the two for 4 hours each during the daytime (henceforth '444 assumption'). This is following the method used in >, which actually uses monthly averages of daily data, and is supposed to be representative of daytime rather than the full diurnal cycle. Daily data were originally used because at the time that the analysis was performed (August 2020), the CEDA archive contained sub-daily data for the variables of interest for only a small number of CMIP6 models.

We compared hazard gradient calculated from 3hd to those calculated from the 444 assumption from monthly data. We did not make any assumption about which of the 3hd time steps represented the daytime, and simply took the daily mean. This means that the 3hd includes nighttime temperatures, whereas 444 does not. Supplementary Figure 3 shows the hazard gradient calculated with monthly data and with 3-hourly data. The Spearman's rank correlation between the two is 0.91. The monthly data captures almost all of the variation in hazard-gradient, as the hazard gradient is mainly driven by large-scale long-term changes in air temperature. Therefore, it is valid to use daily or even monthly data for this analysis.

In order to examine the assumption about radiation, we used surface down-welling shortwave radiation (CMIP6 variable 'rsds'), to estimate the black-globe temperature (BGT) following the method described in Gaspar and Quintela (2009)>. To simplify the calculation, we assumed that the effective temperature of the sky is the equal to the surface air temperature, and neglected up-going radiation. Daily average data would not capture important sub-daily variation in rsds. Values were calculated for land grid cells between latitude [-10.6, 53.1] deg N, longitude [27.2, 153] deg E, which covers the area identified as Asia in the RiceAtlas dataset. Down-welling shortwave radiation in this climate model is an instantaneous variable, so was linearly interpolated to the time interval of the other variables. WBGT calculated using the shade assumption will be called WBGTshade, WBGT calculated using rsds will be called WBGTr. Monthly-average labour-impact metrics and hazard gradients were calculated from WBGTr and WBGTshade, and were compared. Spearman's rank correlation coefficient was calculated.

WBGTr is always greater than or equal to WBGTshade because BGT is always greater than or equal to the effective temperature of the sky. Monthly-average labour impact metrics calculated with WBGTr were therefore always greater than or equal to WBGTshade. The monthly-average labour-impact metric calculated with WBGTr is up to 2.8 % greater than with WBGTshade. Supplementary Figure 4 shows maps of the seasonal average difference between the labour-impact metric calculated using WBGTr and WBGTshade. Using radiation produces sub-daily and seasonal variation in the calculated WBGT. However, this has negligible effects on the hazard-gradient because there is no long-term trend in the difference between WBGTshade and WBGTr. Supplementary Figure 5 is a scatter plot of hazard-gradient, calculated with WBGTr and WBGTshade, averaged by rice harvest season (as in Figure 6 of the main text), showing that the hazard-gradient calculated with and without radiation are almost equal. The Spearman's rank correlation between the monthly-average labour-impact metric calculated with and without radiation is 0.99, and between the hazard-gradients 0.99.

In conclusion, the long-term trend in air temperature is very strong, whereas variation on shorter timescales, coming from daily variation and radiation, is smoothed out by averaging. We note also that surface radiation is one of the most uncertain aspects of global climate models. Radiation is important for human heat stress, but the long-term, large-scale trend in average WBGT is driven by changes in air temperature.

2.2 Labour-impact metrics

To examine the difference made by the assumed labour-impact metric, we reproduced the plots with different labour impact metrics. The different metrics are plotted in Supplementary Figure 8.

The labour impact-equations are as follows: Dunne $25 * (\mathrm{maximum}(0., \mathrm{WBGT} - 25)) ** (2/3))$, HOTHAPS $100 - 100 * (0.1 + (0.9/(1 + (WBGT/30.94) ** 16.64)))$. All equations are clipped to the range [0, 100], and are in units of %.

The impact-metric used by Dunne et al. (2013)> is based on regulatory standards for occupational health. The results using this impact-metric are plotted against the results calculated using the impact-metric from Sahu et al (2013)[5] in Supplementary Figure 6. The two functions have a low threshold at a similar value, and the upper threshold is rarely reached for both metrics, but the average gradient of the Dunne et al. (2013) metric is higher.

The other labour-impact metric we evaluated was the HOTHAPS high-intensity function. This is used by Orlov et al. (2020)> to represent labour in the crop sector. This impact-metric is compared to that from Sahu et al(2013) in Supplementary Figure 7. Because of the S-curve form of this labour-impact function, different parts of the WBGT distribution are emphasised. The Sahu et al (2013) function gives equal weight to all WBGT > 23 C, whereas the HOTHAPS high-intensity function emphasises WBGT close to 31 C. This makes consideration of seasonal variation even more important.

The Asia-wide trend against GSAT of both of these rice-weighted metrics has coefficient of determination R>0.96, and gradient t-test p value <<0.01. In all cases, the long-term trends in heat-stress are determined by changes in air-temperature.

Basic results are compatible with those of other studies. Orlov et al. (2020) projected a decrease in work productivity of approximately 18% and 17% for South Asia and Southeast Asia respectively, in the crop sector by 2100 under the CMIP5 high-emission scenario. We were able to reproduce similar results by using the labour impact relationship they used, and weighting by population density>: multi-model mean (standard deviation) 14(5)% and 17(8)% change between the decade starting 2015 and the decade starting 2090 in SSP585 (a CMIP6 high emissions scenario) for South Asia and Southeast Asia respectively. Using the relationship in Dunne et al. (2013), these numbers are 22(5)% and 29(8)%.

Supplementary table 1: Subnational locations mentioned in text

Location name	Hierarchical administrative subdivision codes (HASC)
Punjab	IN.PB
Haryana	IN.HR
Kerala	IN.KL
West Bengal	IN.WB

The full list of locations used in the analysis can be found in the data supplement.

References

1. Laborte, A. G. *et al.* RiceAtlas, a spatial database of global rice calendars and production. *Sci. Data* **4**, 1–10 (2017).

2. Kjellstrom, T., Freyberg, C., Lemke, B., Otto, M. & Briggs, D. Estimating population heat exposure and impacts on working people in conjunction with climate change. *Int. J. Biometeorol.* **62**, 291–306 (2018).

3. Gaspar, A. R. & Quintela, D. A. Physical modelling of globe and natural wet bulb temperatures to predict WBGT heat stress index in outdoor environments. *Int. J. Biometeorol.* **53**, 221–230 (2009).

4. Dunne, J. P., Stouffer, R. J. & John, J. G. Reductions in labour capacity from heat stress under climate warming. *Nat. Clim. Chang.* **3**, 563–566 (2013).

5. Sahu, S., Sett, M. & Kjellstrom, T. Heat Exposure, Cardiovascular Stress and Work Productivity in Rice Harvesters in India: Implications for a Climate Change Future. *Ind. Health* **51**, 424–431 (2013).

6. Orlov, A., Sillmann, J., Aunan, K., Kjellstrom, T. & Aaheim, A. Economic costs of heat-induced reductions in worker productivity due to global warming. *Glob. Environ. Chang.* **63**, (2020).

7. Center for International Earth Science Information Network Columbia University. Gridded Population of the World, Version 4. doi:10.7927/H4F47M65.

Supplementary Figures

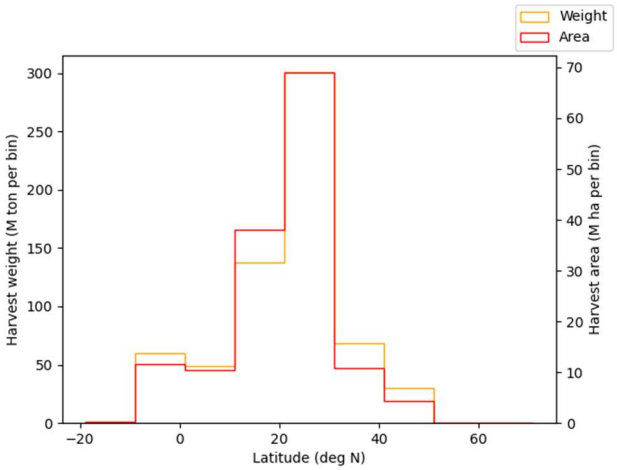

Supplementary Figure 1: Rice harvest weight and area in Asia, plotted in latitude bins. Data from RiceAtlas.

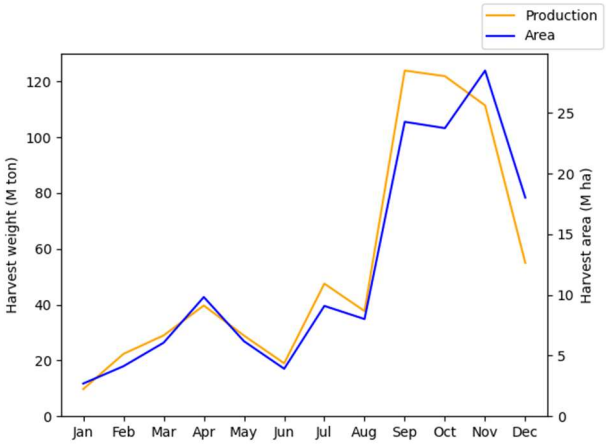

Supplementary Figure 2: Rice harvest weight and area in Asia, plotted against month. Data from RiceAtlas.

1

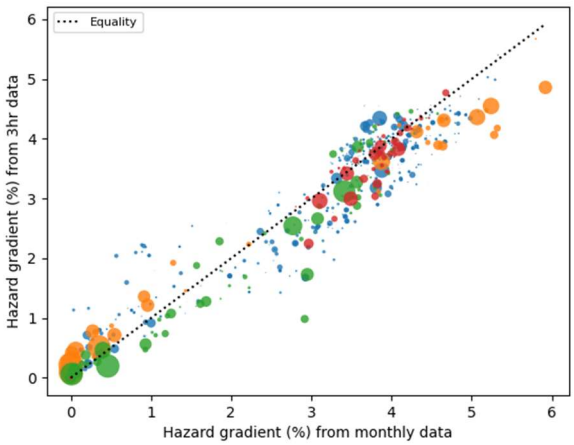

Supplementary Figure 3: Scatter plot, with marker size proportional to total harvest weight, showing hazard gradient calculated with monthly and 3-hourly CMIP6 data for a single model (HadGEM-GC31-LL SSP245). Colours have the same meaning as in the other plots.

1

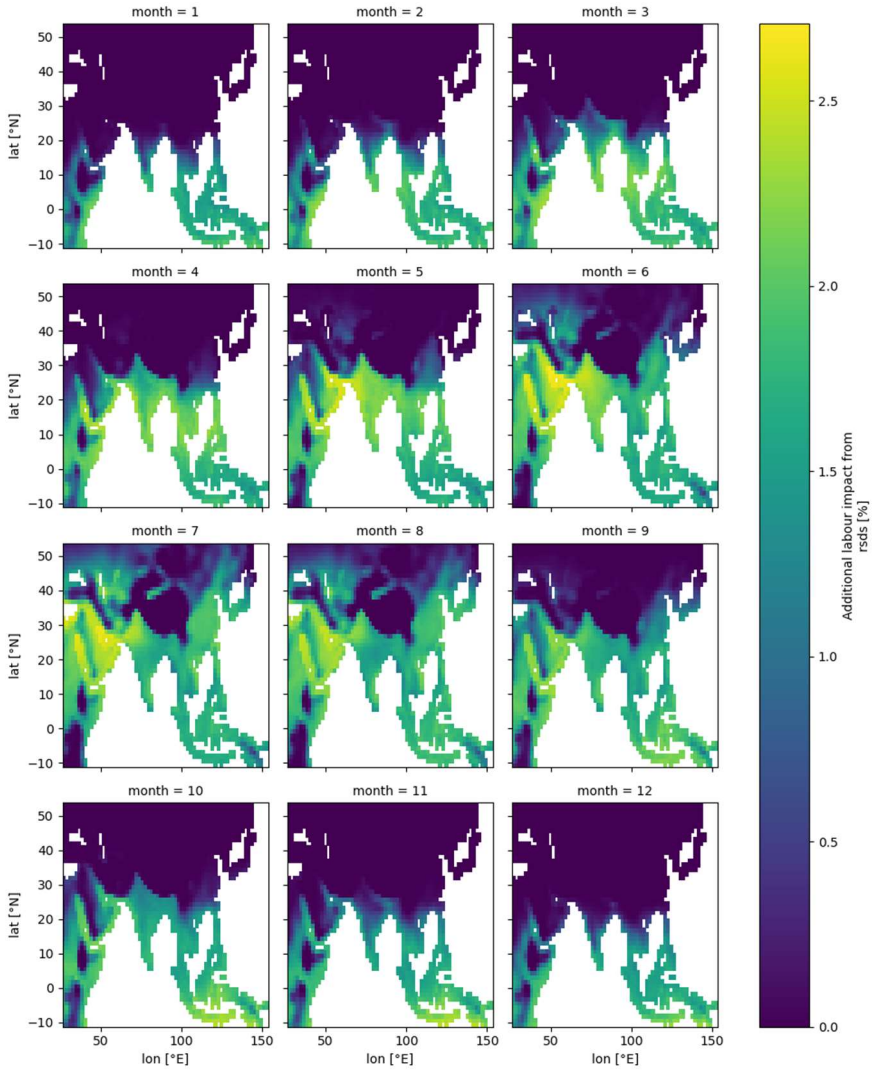

Supplementary Figure 4: Additional labour-impact caused by including shortwave radiation in the WBGT calculation in HadGEM-GC31-LL SSP245.

1

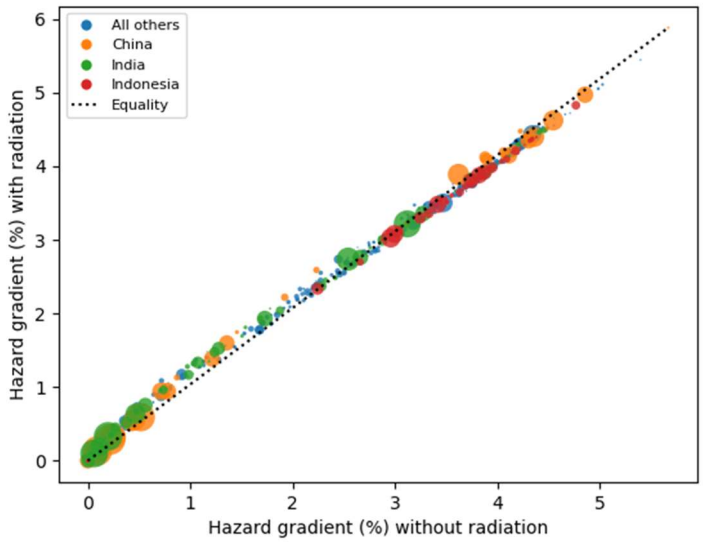

Supplementary Figure 5: Scatter plot, with marker size proportional to total harvest weight, showing hazard gradient calculated with and without radiation, from 3-hourly CMIP6 data for a single model (HadGEM-GC31-LL SSP245). Colours identify points belonging to China, India, and Indonesia. Hazard gradient calculated with and without gradient are close to equal.

2

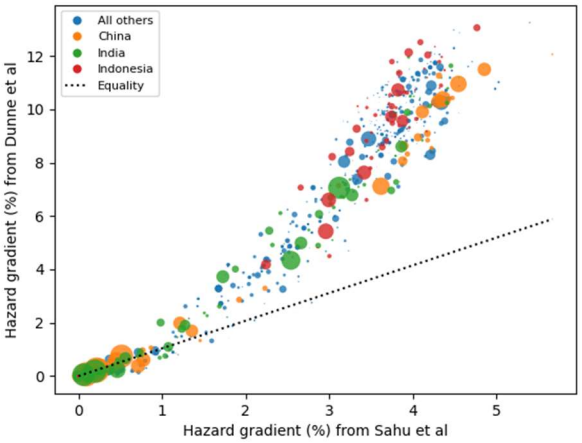

Supplementary Figure 6: Scatter plot, with marker size proportional to total harvest weight, showing hazard gradient calculated, from 3-hourly CMIP6 data for a single model (HadGEM-GC31-LL SSP245) with different labour impact metrics. The function from Sahu et al is compared to the function of Dunne et al. Colours identify points belonging to China, India, and Indonesia

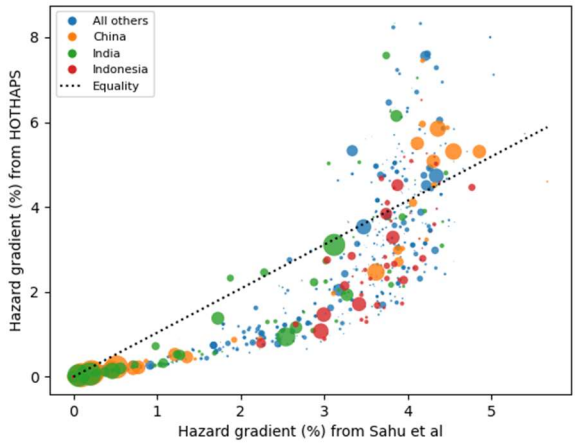

Supplementary Figure 7: Scatter plot, with marker size proportional to total harvest weight, showing hazard gradient calculated, from 3-hourly CMIP6 data for a single model (HadGEM-GC31-LL SSP245) with different labour impact metrics. The function from Sahu et al is compared to the HOTHAPS high-intensity function. Colours identify points belonging to China, India, and Indonesia

1

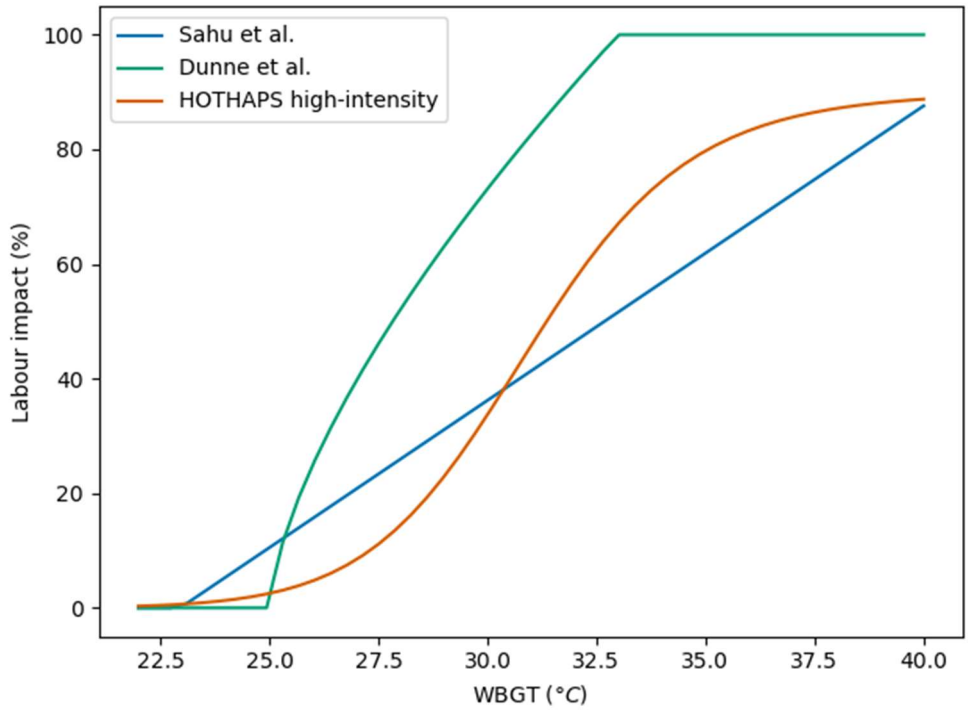

Supplementary Figure 8: Different labour impact metrics to be compared.

2

Supplementary Tables

Supplementary table 2: CMIP6 climate models used

ACCESS-CM2

ACCESS-ESM1-5
CanESM5
FGOALS-g3
GFDL-CM4
HadGEM3-GC31-LL
INM-CM4-8
INM-CM5-0
MIROC6
MPI-ESM1-2-HR
MPI-ESM1-2-LR
MRI-ESM2-0
NorESM2-MM
UKESM1-0-LL

Supplementary table 3: CMIP6 data citations

Centre	Model	Experiment	Citation
CAS	FGOALS-g3	historical	Li, L. (2019). CAS FGOALS-g3 model output prepared for CMIP6 CMIP historical. v20190826. Earth System Grid Federation. https://doi.org/10.22033/ESGF/CMIP6.3356
CAS	FGOALS-g3	ssp370	Li, L. (2019). CAS FGOALS-g3 model output prepared for CMIP6 ScenarioMIP ssp370. v20190820. Earth System Grid Federation. https://doi.org/10.22033/ESGF/CMIP6.3480
CCCma	CanESM5	historical	Swart, N.C., Cole, J.N.S., Kharin, V.V., Lazare, M., Scinocca, J.F., Gillett, N.P., Anstey, J., Arora, V., Christian, J.R., Jiao, Y., Lee, W.G., Majaess, F., Saenko, O.A., Seiler, C., Seinen, C., Shao, A., Solheim, L., von Salzen, K., Yang, D., Winter, B., Sigmond, M. (2019). CCCma CanESM5 model output prepared for CMIP6 CMIP historical. v20190429. Earth System Grid Federation. https://doi.org/10.22033/ESGF/CMIP6.3610
CCCma	CanESM5	ssp119	Swart, N.C., Cole, J.N.S., Kharin, V.V., Lazare, M., Scinocca, J.F., Gillett, N.P., Anstey, J., Arora, V., Christian, J.R., Jiao, Y., Lee, W.G., Majaess, F., Saenko, O.A., Seiler, C., Seinen, C., Shao, A., Solheim, L., von Salzen, K., Yang, D., Winter, B., Sigmond, M. (2019). CCCma CanESM5 model output prepared for CMIP6 ScenarioMIP ssp119. v20190429. Earth System Grid Federation. https://doi.org/10.22033/ESGF/CMIP6.3682
CCCma	CanESM5	ssp126	Swart, N.C., Cole, J.N.S., Kharin, V.V., Lazare, M., Scinocca, J.F., Gillett, N.P., Anstey, J., Arora, V., Christian, J.R., Jiao, Y., Lee, W.G., Majaess, F., Saenko, O.A., Seiler, C., Seinen, C., Shao, A., Solheim, L., von Salzen, K., Yang, D., Winter, B., Sigmond, M. (2019). CCCma CanESM5 model output prepared for CMIP6

			ScenarioMIP ssp126. v20190429. Earth System Grid Federation. https://doi.org/10.22033/ESGF/CMIP6.3683
CCCma	CanESM5	ssp245	Swart, N.C., Cole, J.N.S., Kharin, V.V., Lazare, M., Scinocca, J.F., Gillett, N.P., Anstey, J., Arora, V., Christian, J.R., Jiao, Y., Lee, W.G., Majaess, F., Saenko, O.A., Seiler, C., Seinen, C., Shao, A., Solheim, L., von Salzen, K., Yang, D., Winter, B., Sigmond, M. (2019). CCCma CanESM5 model output prepared for CMIP6 ScenarioMIP ssp245. v20190429. Earth System Grid Federation. https://doi.org/10.22033/ESGF/CMIP6.3685
CCCma	CanESM5	ssp370	Swart, N.C., Cole, J.N.S., Kharin, V.V., Lazare, M., Scinocca, J.F., Gillett, N.P., Anstey, J., Arora, V., Christian, J.R., Jiao, Y., Lee, W.G., Majaess, F., Saenko, O.A., Seiler, C., Seinen, C., Shao, A., Solheim, L., von Salzen, K., Yang, D., Winter, B., Sigmond, M. (2019). CCCma CanESM5 model output prepared for CMIP6 ScenarioMIP ssp370. v20190429. Earth System Grid Federation. https://doi.org/10.22033/ESGF/CMIP6.3690
CCCma	CanESM5	ssp434	Swart, N.C., Cole, J.N.S., Kharin, V.V., Lazare, M., Scinocca, J.F., Gillett, N.P., Anstey, J., Arora, V., Christian, J.R., Jiao, Y., Lee, W.G., Majaess, F., Saenko, O.A., Seiler, C., Seinen, C., Shao, A., Solheim, L., von Salzen, K., Yang, D., Winter, B., Sigmond, M. (2019). CCCma CanESM5 model output prepared for CMIP6 ScenarioMIP ssp434. v20190429. Earth System Grid Federation. https://doi.org/10.22033/ESGF/CMIP6.3692
CCCma	CanESM5	ssp460	Swart, N.C., Cole, J.N.S., Kharin, V.V., Lazare, M., Scinocca, J.F., Gillett, N.P., Anstey, J., Arora, V., Christian, J.R., Jiao, Y., Lee, W.G., Majaess, F., Saenko, O.A., Seiler, C., Seinen, C., Shao, A., Solheim, L., von Salzen, K., Yang, D., Winter, B., Sigmond, M. (2019). CCCma CanESM5 model output prepared for CMIP6 ScenarioMIP ssp460. v20190429. Earth System Grid Federation. https://doi.org/10.22033/ESGF/CMIP6.3693
CCCma	CanESM5	ssp534-over	Swart, N.C., Cole, J.N.S., Kharin, V.V., Lazare, M., Scinocca, J.F., Gillett, N.P., Anstey, J., Arora, V., Christian, J.R., Jiao, Y., Lee, W.G., Majaess, F., Saenko, O.A., Seiler, C., Seinen, C., Shao, A., Solheim, L., von Salzen, K., Yang, D., Winter, B., Sigmond, M. (2019). CCCma CanESM5 model output prepared for CMIP6 ScenarioMIP ssp534-over. v20190429. Earth System Grid Federation. https://doi.org/10.22033/ESGF/CMIP6.3694

CCCma	CanESM5	ssp585	Swart, N.C., Cole, J.N.S., Kharin, V.V., Lazare, M., Scinocca, J.F., Gillett, N.P., Anstey, J., Arora, V., Christian, J.R., Jiao, Y., Lee, W.G., Majaess, F., Saenko, O.A., Seiler, C., Seinen, C., Shao, A., Solheim, L., von Salzen, K., Yang, D., Winter, B., Sigmond, M. (2019). CCCma CanESM5 model output prepared for CMIP6 ScenarioMIP ssp585. v20190429. Earth System Grid Federation. https://doi.org/10.22033/ESGF/CMIP6.3696
CNRM-CERFACS	CNRM-CM6-1	historical	Voldoire, A. (2018). CNRM-CERFACS CNRM-CM6-1 model output prepared for CMIP6 CMIP historical. v20180917. Earth System Grid Federation. https://doi.org/10.22033/ESGF/CMIP6.4066
CNRM-CERFACS	CNRM-CM6-1	ssp126	Voldoire, A. (2019). CNRM-CERFACS CNRM-CM6-1 model output prepared for CMIP6 ScenarioMIP ssp126. v20190219. Earth System Grid Federation. https://doi.org/10.22033/ESGF/CMIP6.4184
CNRM-CERFACS	CNRM-CM6-1	ssp245	Voldoire, A. (2019). CNRM-CERFACS CNRM-CM6-1 model output prepared for CMIP6 ScenarioMIP ssp245. v20190219. Earth System Grid Federation. https://doi.org/10.22033/ESGF/CMIP6.4189
CNRM-CERFACS	CNRM-CM6-1	ssp370	Voldoire, A. (2019). CNRM-CERFACS CNRM-CM6-1 model output prepared for CMIP6 ScenarioMIP ssp370. v20190219. Earth System Grid Federation. https://doi.org/10.22033/ESGF/CMIP6.4197
CNRM-CERFACS	CNRM-CM6-1	ssp585	Voldoire, A. (2019). CNRM-CERFACS CNRM-CM6-1 model output prepared for CMIP6 ScenarioMIP ssp585. v20190219. Earth System Grid Federation. https://doi.org/10.22033/ESGF/CMIP6.4224
CSIRO	ACCESS-ESM1-5	historical	Ziehn, T., Chamberlain, M., Lenton, A., Law, R., Bodman, R., Dix, M., Wang, Y., Dobrohotoff, P., Srbinovsky, J., Stevens, L., Vohralik, P., Mackallah, C., Sullivan, A., O'Farrell, S., Druken, K. (2019). CSIRO ACCESS-ESM1-5 model output prepared for CMIP6 CMIP historical. v20191115. Earth System Grid Federation. https://doi.org/10.22033/ESGF/CMIP6.4272
CSIRO	ACCESS-ESM1-5	ssp126	Ziehn, T., Chamberlain, M., Lenton, A., Law, R., Bodman, R., Dix, M., Wang, Y., Dobrohotoff, P., Srbinovsky, J., Stevens, L., Vohralik, P., Mackallah, C., Sullivan, A., O'Farrell, S., Druken, K. (2019). CSIRO ACCESS-ESM1-5 model output prepared for CMIP6 ScenarioMIP ssp126. v20191115. Earth System Grid Federation. https://doi.org/10.22033/ESGF/CMIP6.4320
CSIRO	ACCESS-ESM1-5	ssp245	Ziehn, T., Chamberlain, M., Lenton, A., Law, R., Bodman, R., Dix, M., Wang, Y., Dobrohotoff, P., Srbinovsky, J., Stevens, L., Vohralik, P., Mackallah, C., Sullivan, A., O'Farrell, S., Druken, K. (2019). CSIRO ACCESS-ESM1-5 model output prepared for CMIP6 ScenarioMIP ssp245. v20191115. Earth System Grid Federation. https://doi.org/10.22033/ESGF/CMIP6.4322

CSIRO	ACCESS-ESM1-5	ssp370	Ziehn, T., Chamberlain, M., Lenton, A., Law, R., Bodman, R., Dix, M., Wang, Y., Dobrohotoff, P., Srbinovsky, J., Stevens, L., Vohralik, P., Mackallah, C., Sullivan, A., O'Farrell, S., Druken, K. (2019). CSIRO ACCESS-ESM1-5 model output prepared for CMIP6 ScenarioMIP ssp370. v20191115. Earth System Grid Federation. https://doi.org/10.22033/ESGF/CMIP6.4324
CSIRO	ACCESS-ESM1-5	ssp585	Ziehn, T., Chamberlain, M., Lenton, A., Law, R., Bodman, R., Dix, M., Wang, Y., Dobrohotoff, P., Srbinovsky, J., Stevens, L., Vohralik, P., Mackallah, C., Sullivan, A., O'Farrell, S., Druken, K. (2019). CSIRO ACCESS-ESM1-5 model output prepared for CMIP6 ScenarioMIP ssp585. v20191115. Earth System Grid Federation. https://doi.org/10.22033/ESGF/CMIP6.4333
CSIRO-ARCCSS	ACCESS-CM2	historical	Dix, M., Bi, D., Dobrohotoff, P., Fiedler, R., Harman, I., Law, R., Mackallah, C., Marsland, S., O'Farrell, S., Rashid, H., Srbinovsky, J., Sullivan, A., Trenham, C., Vohralik, P., Watterson, I., Williams, G., Woodhouse, M., Bodman, R., Dias, F.B., Domingues, C., Hannah, N., Heerdegen, A., Savita, A., Wales, S., Allen, C., Druken, K., Evans, B., Richards, C., Ridzwan, S.M., Roberts, D., Smillie, J., Snow, K., Ward, M., Yang, R. (2019). CSIRO-ARCCSS ACCESS-CM2 model output prepared for CMIP6 CMIP historical. v20191108. Earth System Grid Federation. https://doi.org/10.22033/ESGF/CMIP6.4271
CSIRO-ARCCSS	ACCESS-CM2	ssp126	Dix, M., Bi, D., Dobrohotoff, P., Fiedler, R., Harman, I., Law, R., Mackallah, C., Marsland, S., O'Farrell, S., Rashid, H., Srbinovsky, J., Sullivan, A., Trenham, C., Vohralik, P., Watterson, I., Williams, G., Woodhouse, M., Bodman, R., Dias, F.B., Domingues, C., Hannah, N., Heerdegen, A., Savita, A., Wales, S., Allen, C., Druken, K., Evans, B., Richards, C., Ridzwan, S.M., Roberts, D., Smillie, J., Snow, K., Ward, M., Yang, R. (2019). CSIRO-ARCCSS ACCESS-CM2 model output prepared for CMIP6 ScenarioMIP ssp126. v20191108. Earth System Grid Federation. https://doi.org/10.22033/ESGF/CMIP6.4319
CSIRO-ARCCSS	ACCESS-CM2	ssp245	Dix, M., Bi, D., Dobrohotoff, P., Fiedler, R., Harman, I., Law, R., Mackallah, C., Marsland, S., O'Farrell, S., Rashid, H., Srbinovsky, J., Sullivan, A., Trenham, C., Vohralik, P., Watterson, I., Williams, G., Woodhouse, M., Bodman, R., Dias, F.B., Domingues, C., Hannah, N., Heerdegen, A., Savita, A., Wales, S., Allen, C., Druken, K., Evans, B., Richards, C., Ridzwan, S.M., Roberts, D., Smillie, J., Snow, K., Ward, M., Yang, R. (2019). CSIRO-ARCCSS ACCESS-CM2 model output prepared for CMIP6 ScenarioMIP ssp245. v20191108. Earth System Grid Federation. https://doi.org/10.22033/ESGF/CMIP6.4321

CSIRO-ARCCSS	ACCESS-CM2	ssp370	Dix, M., Bi, D., Dobrohotoff, P., Fiedler, R., Harman, I., Law, R., Mackallah, C., Marsland, S., O'Farrell, S., Rashid, H., Srbinovsky, J., Sullivan, A., Trenham, C., Vohralik, P., Watterson, I., Williams, G., Woodhouse, M., Bodman, R., Dias, F.B., Domingues, C., Hannah, N., Heerdegen, A., Savita, A., Wales, S., Allen, C., Druken, K., Evans, B., Richards, C., Ridzwan, S.M., Roberts, D., Smillie, J., Snow, K., Ward, M., Yang, R. (2019). CSIRO-ARCCSS ACCESS-CM2 model output prepared for CMIP6 ScenarioMIP ssp370. v20191108. Earth System Grid Federation. https://doi.org/10.22033/ESGF/CMIP6.4323
CSIRO-ARCCSS	ACCESS-CM2	ssp585	Dix, M., Bi, D., Dobrohotoff, P., Fiedler, R., Harman, I., Law, R., Mackallah, C., Marsland, S., O'Farrell, S., Rashid, H., Srbinovsky, J., Sullivan, A., Trenham, C., Vohralik, P., Watterson, I., Williams, G., Woodhouse, M., Bodman, R., Dias, F.B., Domingues, C., Hannah, N., Heerdegen, A., Savita, A., Wales, S., Allen, C., Druken, K., Evans, B., Richards, C., Ridzwan, S.M., Roberts, D., Smillie, J., Snow, K., Ward, M., Yang, R. (2019). CSIRO-ARCCSS ACCESS-CM2 model output prepared for CMIP6 ScenarioMIP ssp585. v20191108. Earth System Grid Federation. https://doi.org/10.22033/ESGF/CMIP6.4332
DKRZ	MPI-ESM1-2-HR	ssp126	Schupfner, M., Wieners, K.H., Wachsmann, F., Steger, C., Bittner, M., Jungclaus, J., FrÃ¼h, B., Pankatz, K., Giorgetta, M., Reick, C., Legutke, S., Esch, M., Gayler, V., Haak, H., de Vrese, P., Raddatz, T., Mauritsen, T., von Storch, J.S., Behrens, J., Brovkin, V., Claussen, M., Crueger, T., Fast, I., Fiedler, S., Hagemann, S., Hohenegger, C., Jahns, T., Kloster, S., Kinne, S., Lasslop, G., Kornblueh, L., Marotzke, J., Matei, D., Meraner, K., Mikolajewicz, U., Modali, K., MÃ¼ller, W., Nabel, J., Notz, D., Peters, K., Pincus, R., Pohlmann, H., Pongratz, J., Rast, S., Schmidt, H., Schnur, R., Schulzweida, U., Six, K., Stevens, B., Voigt, A., Roeckner, E. (2019). DKRZ MPI-ESM1-2-HR model output prepared for CMIP6 ScenarioMIP ssp126. v20190710. Earth System Grid Federation. https://doi.org/10.22033/ESGF/CMIP6.4397
DKRZ	MPI-ESM1-2-HR	ssp245	Schupfner, M., Wieners, K.H., Wachsmann, F., Steger, C., Bittner, M., Jungclaus, J., FrÃ¼h, B., Pankatz, K., Giorgetta, M., Reick, C., Legutke, S., Esch, M., Gayler, V., Haak, H., de Vrese, P., Raddatz, T., Mauritsen, T., von Storch, J.S., Behrens, J., Brovkin, V., Claussen, M., Crueger, T., Fast, I., Fiedler, S., Hagemann, S., Hohenegger, C., Jahns, T., Kloster, S., Kinne, S., Lasslop, G., Kornblueh, L., Marotzke, J., Matei, D., Meraner, K., Mikolajewicz, U., Modali, K., MÃ¼ller, W., Nabel, J., Notz, D., Peters, K., Pincus, R., Pohlmann, H., Pongratz, J., Rast, S., Schmidt, H., Schnur, R., Schulzweida, U., Six, K., Stevens, B., Voigt, A., Roeckner, E. (2019). DKRZ MPI-ESM1-2-HR model output prepared for CMIP6

			ScenarioMIP ssp245. v20190710. Earth System Grid Federation. https://doi.org/10.22033/ESGF/CMIP6.4398
DKRZ	MPI-ESM1-2-HR	ssp370	Schupfner, M., Wieners, K.H., Wachsmann, F., Steger, C., Bittner, M., Jungclaus, J., FrÃ¼h, B., Pankatz, K., Giorgetta, M., Reick, C., Legutke, S., Esch, M., Gayler, V., Haak, H., de Vrese, P., Raddatz, T., Mauritsen, T., von Storch, J.S., Behrens, J., Brovkin, V., Claussen, M., Crueger, T., Fast, I., Fiedler, S., Hagemann, S., Hohenegger, C., Jahns, T., Kloster, S., Kinne, S., Lasslop, G., Kornblueh, L., Marotzke, J., Matei, D., Meraner, K., Mikolajewicz, U., Modali, K., MÃ¼ller, W., Nabel, J., Notz, D., Peters, K., Pincus, R., Pohlmann, H., Pongratz, J., Rast, S., Schmidt, H., Schnur, R., Schulzweida, U., Six, K., Stevens, B., Voigt, A., Roeckner, E. (2019). DKRZ MPI-ESM1-2-HR model output prepared for CMIP6 ScenarioMIP ssp370. v20190710. Earth System Grid Federation. https://doi.org/10.22033/ESGF/CMIP6.4399
DKRZ	MPI-ESM1-2-HR	ssp585	Schupfner, M., Wieners, K.H., Wachsmann, F., Steger, C., Bittner, M., Jungclaus, J., FrÃ¼h, B., Pankatz, K., Giorgetta, M., Reick, C., Legutke, S., Esch, M., Gayler, V., Haak, H., de Vrese, P., Raddatz, T., Mauritsen, T., von Storch, J.S., Behrens, J., Brovkin, V., Claussen, M., Crueger, T., Fast, I., Fiedler, S., Hagemann, S., Hohenegger, C., Jahns, T., Kloster, S., Kinne, S., Lasslop, G., Kornblueh, L., Marotzke, J., Matei, D., Meraner, K., Mikolajewicz, U., Modali, K., MÃ¼ller, W., Nabel, J., Notz, D., Peters, K., Pincus, R., Pohlmann, H., Pongratz, J., Rast, S., Schmidt, H., Schnur, R., Schulzweida, U., Six, K., Stevens, B., Voigt, A., Roeckner, E. (2019). DKRZ MPI-ESM1-2-HR model output prepared for CMIP6 ScenarioMIP ssp585. v20190710. Earth System Grid Federation. https://doi.org/10.22033/ESGF/CMIP6.4403
INM	INM-CM4-8	historical	Volodin, E., Mortikov, E., Gritsun, A., Lykossov, V., Galin, V., Diansky, N., Gusev, A., Kostrykin, S., Iakovlev, N., Shestakova, A., Emelina, S. (2019). INM INM-CM4-8 model output prepared for CMIP6 CMIP historical. v20190530. Earth System Grid Federation. https://doi.org/10.22033/ESGF/CMIP6.5069
INM	INM-CM4-8	ssp126	Volodin, E., Mortikov, E., Gritsun, A., Lykossov, V., Galin, V., Diansky, N., Gusev, A., Kostrykin, S., Iakovlev, N., Shestakova, A., Emelina, S. (2019). INM INM-CM4-8 model output prepared for CMIP6 ScenarioMIP ssp126.

			v20190603. Earth System Grid Federation. https://doi.org/10.22033/ESGF/CMIP6.12325
INM	INM-CM4-8	ssp370	Volodin, E., Mortikov, E., Gritsun, A., Lykossov, V., Galin, V., Diansky, N., Gusev, A., Kostrykin, S., Iakovlev, N., Shestakova, A., Emelina, S. (2019). INM INM-CM4-8 model output prepared for CMIP6 ScenarioMIP ssp370. v20190603. Earth System Grid Federation. https://doi.org/10.22033/ESGF/CMIP6.12329
INM	INM-CM4-8	ssp585	Volodin, E., Mortikov, E., Gritsun, A., Lykossov, V., Galin, V., Diansky, N., Gusev, A., Kostrykin, S., Iakovlev, N., Shestakova, A., Emelina, S. (2019). INM INM-CM4-8 model output prepared for CMIP6 ScenarioMIP ssp585. v20190603. Earth System Grid Federation. https://doi.org/10.22033/ESGF/CMIP6.12337
INM	INM-CM5-0	historical	Volodin, E., Mortikov, E., Gritsun, A., Lykossov, V., Galin, V., Diansky, N., Gusev, A., Kostrykin, S., Iakovlev, N., Shestakova, A., Emelina, S. (2019). INM INM-CM5-0 model output prepared for CMIP6 CMIP historical. v20190610. Earth System Grid Federation. https://doi.org/10.22033/ESGF/CMIP6.5070
INM	INM-CM5-0	ssp126	Volodin, E., Mortikov, E., Gritsun, A., Lykossov, V., Galin, V., Diansky, N., Gusev, A., Kostrykin, S., Iakovlev, N., Shestakova, A., Emelina, S. (2019). INM INM-CM5-0 model output prepared for CMIP6 ScenarioMIP ssp126. v20190619. Earth System Grid Federation. https://doi.org/10.22033/ESGF/CMIP6.12326
INM	INM-CM5-0	ssp370	Volodin, E., Mortikov, E., Gritsun, A., Lykossov, V., Galin, V., Diansky, N., Gusev, A., Kostrykin, S., Iakovlev, N., Shestakova, A., Emelina, S. (2019). INM INM-CM5-0 model output prepared for CMIP6 ScenarioMIP ssp370. v20190618. Earth System Grid Federation. https://doi.org/10.22033/ESGF/CMIP6.12330
INM	INM-CM5-0	ssp585	Volodin, E., Mortikov, E., Gritsun, A., Lykossov, V., Galin, V., Diansky, N., Gusev, A., Kostrykin, S., Iakovlev, N., Shestakova, A., Emelina, S. (2019). INM INM-CM5-0 model output prepared for CMIP6 ScenarioMIP ssp585. v20190724. Earth System Grid Federation. https://doi.org/10.22033/ESGF/CMIP6.12338
MIROC	MIROC6	historical	Tatebe, H., Watanabe, M. (2018). MIROC MIROC6 model output prepared for CMIP6 CMIP historical. v20191016. Earth System Grid Federation. https://doi.org/10.22033/ESGF/CMIP6.5603
MIROC	MIROC6	ssp119	Shiogama, H., Abe, M., Tatebe, H. (2019). MIROC MIROC6 model output prepared for CMIP6 ScenarioMIP ssp119. v20191016. Earth System Grid Federation. https://doi.org/10.22033/ESGF/CMIP6.5741
MIROC	MIROC6	ssp126	Shiogama, H., Abe, M., Tatebe, H. (2019). MIROC MIROC6 model output prepared for CMIP6 ScenarioMIP

			ssp126. v20191016. Earth System Grid Federation. https://doi.org/10.22033/ESGF/CMIP6.5743
MIROC	MIROC6	ssp370	Shiogama, H., Abe, M., Tatebe, H. (2019). MIROC MIROC6 model output prepared for CMIP6 ScenarioMIP ssp370. v20191016. Earth System Grid Federation. https://doi.org/10.22033/ESGF/CMIP6.5752
MIROC	MIROC6	ssp434	Shiogama, H., Abe, M., Tatebe, H. (2019). MIROC MIROC6 model output prepared for CMIP6 ScenarioMIP ssp434. v20191016. Earth System Grid Federation. https://doi.org/10.22033/ESGF/CMIP6.5764
MIROC	MIROC6	ssp460	Shiogama, H., Abe, M., Tatebe, H. (2019). MIROC MIROC6 model output prepared for CMIP6 ScenarioMIP ssp460. v20191016. Earth System Grid Federation. https://doi.org/10.22033/ESGF/CMIP6.5766
MIROC	MIROC6	ssp534-over	Shiogama, H., Abe, M., Tatebe, H. (2019). MIROC MIROC6 model output prepared for CMIP6 ScenarioMIP ssp534-over. v20191016. Earth System Grid Federation. https://doi.org/10.22033/ESGF/CMIP6.5768
MIROC	MIROC6	ssp585	Shiogama, H., Abe, M., Tatebe, H. (2019). MIROC MIROC6 model output prepared for CMIP6 ScenarioMIP ssp585. v20191016. Earth System Grid Federation. https://doi.org/10.22033/ESGF/CMIP6.5771
MOHC	HadGEM3-GC31-LL	historical	Ridley, J., Menary, M., Kuhlbrodt, T., Andrews, M., Andrews, T. (2019). MOHC HadGEM3-GC31-LL model output prepared for CMIP6 CMIP historical. v20190624. Earth System Grid Federation. https://doi.org/10.22033/ESGF/CMIP6.6109
MOHC	HadGEM3-GC31-LL	ssp126	Good, P. (2020). MOHC HadGEM3-GC31-LL model output prepared for CMIP6 ScenarioMIP ssp126. v20200114. Earth System Grid Federation. https://doi.org/10.22033/ESGF/CMIP6.10849
MOHC	HadGEM3-GC31-LL	ssp245	Good, P. (2019). MOHC HadGEM3-GC31-LL model output prepared for CMIP6 ScenarioMIP ssp245. v20190908. Earth System Grid Federation. https://doi.org/10.22033/ESGF/CMIP6.10851
MOHC	HadGEM3-GC31-LL	ssp585	Good, P. (2020). MOHC HadGEM3-GC31-LL model output prepared for CMIP6 ScenarioMIP ssp585. v20200114. Earth System Grid Federation. https://doi.org/10.22033/ESGF/CMIP6.10901
MOHC	UKESM1-0-LL	historical	Tang, Y., Rumbold, S., Ellis, R., Kelley, D., Mulcahy, J., Sellar, A., Walton, J., Jones, C. (2019). MOHC UKESM1-0-LL model output prepared for CMIP6 CMIP historical. v20191209. Earth System Grid Federation. https://doi.org/10.22033/ESGF/CMIP6.6113
MOHC	UKESM1-0-LL	ssp119	Good, P., Sellar, A., Tang, Y., Rumbold, S., Ellis, R., Kelley, D., Kuhlbrodt, T. (2019). MOHC UKESM1-0-LL model output prepared for CMIP6 ScenarioMIP ssp119. v20190830. Earth System Grid Federation. https://doi.org/10.22033/ESGF/CMIP6.6329

MOHC	UKESM1-0-LL	ssp126	Good, P., Sellar, A., Tang, Y., Rumbold, S., Ellis, R., Kelley, D., Kuhlbrodt, T. (2019). MOHC UKESM1-0-LL model output prepared for CMIP6 ScenarioMIP ssp126. v20190708. Earth System Grid Federation. https://doi.org/10.22033/ESGF/CMIP6.6333
MOHC	UKESM1-0-LL	ssp245	Good, P., Sellar, A., Tang, Y., Rumbold, S., Ellis, R., Kelley, D., Kuhlbrodt, T. (2019). MOHC UKESM1-0-LL model output prepared for CMIP6 ScenarioMIP ssp245. v20190715. Earth System Grid Federation. https://doi.org/10.22033/ESGF/CMIP6.6339
MOHC	UKESM1-0-LL	ssp370	Good, P., Sellar, A., Tang, Y., Rumbold, S., Ellis, R., Kelley, D., Kuhlbrodt, T. (2019). MOHC UKESM1-0-LL model output prepared for CMIP6 ScenarioMIP ssp370. v20190726. Earth System Grid Federation. https://doi.org/10.22033/ESGF/CMIP6.6347
MOHC	UKESM1-0-LL	ssp434	Good, P., Sellar, A., Tang, Y., Rumbold, S., Ellis, R., Kelley, D., Kuhlbrodt, T. (2019). MOHC UKESM1-0-LL model output prepared for CMIP6 ScenarioMIP ssp434. v20190828. Earth System Grid Federation. https://doi.org/10.22033/ESGF/CMIP6.6389
MOHC	UKESM1-0-LL	ssp534-over	Good, P., Sellar, A., Tang, Y., Rumbold, S., Ellis, R., Kelley, D., Kuhlbrodt, T. (2019). MOHC UKESM1-0-LL model output prepared for CMIP6 ScenarioMIP ssp534-over. v20190830. Earth System Grid Federation. https://doi.org/10.22033/ESGF/CMIP6.6397
MOHC	UKESM1-0-LL	ssp585	Good, P., Sellar, A., Tang, Y., Rumbold, S., Ellis, R., Kelley, D., Kuhlbrodt, T. (2019). MOHC UKESM1-0-LL model output prepared for CMIP6 ScenarioMIP ssp585. v20190726. Earth System Grid Federation. https://doi.org/10.22033/ESGF/CMIP6.6405
MPI-M	MPI-ESM1-2-HR	historical	Jungclaus, J., Bittner, M., Wieners, K.H., Wachsmann, F., Schupfner, M., Legutke, S., Giorgetta, M., Reick, C., Gayler, V., Haak, H., de Vrese, P., Raddatz, T., Esch, M., Mauritsen, T., von Storch, J.S., Behrens, J., Brovkin, V., Claussen, M., Crueger, T., Fast, I., Fiedler, S., Hagemann, S., Hohenegger, C., Jahns, T., Kloster, S., Kinne, S., Lasslop, G., Kornblueh, L., Marotzke, J., Matei, D., Meraner, K., Mikolajewicz, U., Modali, K., MÃ¼ller, W., Nabel, J., Notz, D., Peters, K., Pincus, R., Pohlmann, H., Pongratz, J., Rast, S., Schmidt, H., Schnur, R., Schulzweida, U., Six, K., Stevens, B., Voigt, A., Roeckner, E. (2019). MPI-M MPI-ESM1-2-HR model output prepared for CMIP6 CMIP historical. v20190710. Earth System Grid Federation. https://doi.org/10.22033/ESGF/CMIP6.6594

MPI-M	MPI-ESM1-2-LR	historical	Wieners, K.H., Giorgetta, M., Jungclaus, J., Reick, C., Esch, M., Bittner, M., Legutke, S., Schupfner, M., Wachsmann, F., Gayler, V., Haak, H., de Vrese, P., Raddatz, T., Mauritsen, T., von Storch, J.S., Behrens, J., Brovkin, V., Claussen, M., Crueger, T., Fast, I., Fiedler, S., Hagemann, S., Hohenegger, C., Jahns, T., Kloster, S., Kinne, S., Lasslop, G., Kornblueh, L., Marotzke, J., Matei, D., Meraner, K., Mikolajewicz, U., Modali, K., MÃ¼ller, W., Nabel, J., Notz, D., Peters, K., Pincus, R., Pohlmann, H., Pongratz, J., Rast, S., Schmidt, H., Schnur, R., Schulzweida, U., Six, K., Stevens, B., Voigt, A., Roeckner, E. (2019). MPI-M MPI-ESM1-2-LR model output prepared for CMIP6 CMIP historical. v20190710. Earth System Grid Federation. https://doi.org/10.22033/ESGF/CMIP6.6595
MPI-M	MPI-ESM1-2-LR	ssp126	Wieners, K.H., Giorgetta, M., Jungclaus, J., Reick, C., Esch, M., Bittner, M., Gayler, V., Haak, H., de Vrese, P., Raddatz, T., Mauritsen, T., von Storch, J.S., Behrens, J., Brovkin, V., Claussen, M., Crueger, T., Fast, I., Fiedler, S., Hagemann, S., Hohenegger, C., Jahns, T., Kloster, S., Kinne, S., Lasslop, G., Kornblueh, L., Marotzke, J., Matei, D., Meraner, K., Mikolajewicz, U., Modali, K., MÃ¼ller, W., Nabel, J., Notz, D., Peters, K., Pincus, R., Pohlmann, H., Pongratz, J., Rast, S., Schmidt, H., Schnur, R., Schulzweida, U., Six, K., Stevens, B., Voigt, A., Roeckner, E. (2019). MPI-M MPI-ESM1-2-LR model output prepared for CMIP6 ScenarioMIP ssp126. v20190710. Earth System Grid Federation. https://doi.org/10.22033/ESGF/CMIP6.6690
MPI-M	MPI-ESM1-2-LR	ssp370	Wieners, K.H., Giorgetta, M., Jungclaus, J., Reick, C., Esch, M., Bittner, M., Legutke, S., Schupfner, M., Wachsmann, F., Gayler, V., Haak, H., de Vrese, P., Raddatz, T., Mauritsen, T., von Storch, J.S., Behrens, J., Brovkin, V., Claussen, M., Crueger, T., Fast, I., Fiedler, S., Hagemann, S., Hohenegger, C., Jahns, T., Kloster, S., Kinne, S., Lasslop, G., Kornblueh, L., Marotzke, J., Matei, D., Meraner, K., Mikolajewicz, U., Modali, K., MÃ¼ller, W., Nabel, J., Notz, D., Peters, K., Pincus, R., Pohlmann, H., Pongratz, J., Rast, S., Schmidt, H., Schnur, R., Schulzweida, U., Six, K., Stevens, B., Voigt, A., Roeckner, E. (2019). MPI-M MPI-ESM1-2-LR model output prepared for CMIP6 ScenarioMIP ssp370. v20190710. Earth System Grid Federation. https://doi.org/10.22033/ESGF/CMIP6.6695

MPI-M	MPI-ESM1-2-LR	ssp585	Wieners, K.H., Giorgetta, M., Jungclaus, J., Reick, C., Esch, M., Bittner, M., Gayler, V., Haak, H., de Vrese, P., Raddatz, T., Mauritsen, T., von Storch, J.S., Behrens, J., Brovkin, V., Claussen, M., Crueger, T., Fast, I., Fiedler, S., Hagemann, S., Hohenegger, C., Jahns, T., Kloster, S., Kinne, S., Lasslop, G., Kornblueh, L., Marotzke, J., Matei, D., Meraner, K., Mikolajewicz, U., Modali, K., MÃ¼ller, W., Nabel, J., Notz, D., Peters, K., Pincus, R., Pohlmann, H., Pongratz, J., Rast, S., Schmidt, H., Schnur, R., Schulzweida, U., Six, K., Stevens, B., Voigt, A., Roeckner, E. (2019). MPI-M MPI-ESM1-2-LR model output prepared for CMIP6 ScenarioMIP ssp585. v20190710. Earth System Grid Federation. https://doi.org/10.22033/ESGF/CMIP6.6705
MRI	MRI-ESM2-0	historical	Yukimoto, S., Koshiro, T., Kawai, H., Oshima, N., Yoshida, K., Urakawa, S., Tsujino, H., Deushi, M., Tanaka, T., Hosaka, M., Yoshimura, H., Shindo, E., Mizuta, R., Ishii, M., Obata, A., Adachi, Y. (2019). MRI MRI-ESM2-0 model output prepared for CMIP6 CMIP historical. v20190603. Earth System Grid Federation. https://doi.org/10.22033/ESGF/CMIP6.6842
MRI	MRI-ESM2-0	ssp119	Yukimoto, S., Koshiro, T., Kawai, H., Oshima, N., Yoshida, K., Urakawa, S., Tsujino, H., Deushi, M., Tanaka, T., Hosaka, M., Yoshimura, H., Shindo, E., Mizuta, R., Ishii, M., Obata, A., Adachi, Y. (2019). MRI MRI-ESM2-0 model output prepared for CMIP6 ScenarioMIP ssp119. v20190603. Earth System Grid Federation. https://doi.org/10.22033/ESGF/CMIP6.6908
MRI	MRI-ESM2-0	ssp126	Yukimoto, S., Koshiro, T., Kawai, H., Oshima, N., Yoshida, K., Urakawa, S., Tsujino, H., Deushi, M., Tanaka, T., Hosaka, M., Yoshimura, H., Shindo, E., Mizuta, R., Ishii, M., Obata, A., Adachi, Y. (2019). MRI MRI-ESM2-0 model output prepared for CMIP6 ScenarioMIP ssp126. v20191108. Earth System Grid Federation. https://doi.org/10.22033/ESGF/CMIP6.6909
MRI	MRI-ESM2-0	ssp245	Yukimoto, S., Koshiro, T., Kawai, H., Oshima, N., Yoshida, K., Urakawa, S., Tsujino, H., Deushi, M., Tanaka, T., Hosaka, M., Yoshimura, H., Shindo, E., Mizuta, R., Ishii, M., Obata, A., Adachi, Y. (2019). MRI MRI-ESM2-0 model output prepared for CMIP6 ScenarioMIP ssp245. v20190603. Earth System Grid Federation. https://doi.org/10.22033/ESGF/CMIP6.6910
MRI	MRI-ESM2-0	ssp370	Yukimoto, S., Koshiro, T., Kawai, H., Oshima, N., Yoshida, K., Urakawa, S., Tsujino, H., Deushi, M., Tanaka, T., Hosaka, M., Yoshimura, H., Shindo, E., Mizuta, R., Ishii, M., Obata, A., Adachi, Y. (2019). MRI MRI-ESM2-0 model output prepared for CMIP6 ScenarioMIP ssp370. v20190603. Earth System Grid Federation. https://doi.org/10.22033/ESGF/CMIP6.6915

MRI	MRI-ESM2-0	ssp434	Yukimoto, S., Koshiro, T., Kawai, H., Oshima, N., Yoshida, K., Urakawa, S., Tsujino, H., Deushi, M., Tanaka, T., Hosaka, M., Yoshimura, H., Shindo, E., Mizuta, R., Ishii, M., Obata, A., Adachi, Y. (2019). MRI MRI-ESM2-0 model output prepared for CMIP6 ScenarioMIP ssp434. v20190603. Earth System Grid Federation. https://doi.org/10.22033/ESGF/CMIP6.6925
MRI	MRI-ESM2-0	ssp460	Yukimoto, S., Koshiro, T., Kawai, H., Oshima, N., Yoshida, K., Urakawa, S., Tsujino, H., Deushi, M., Tanaka, T., Hosaka, M., Yoshimura, H., Shindo, E., Mizuta, R., Ishii, M., Obata, A., Adachi, Y. (2019). MRI MRI-ESM2-0 model output prepared for CMIP6 ScenarioMIP ssp460. v20190603. Earth System Grid Federation. https://doi.org/10.22033/ESGF/CMIP6.6926
MRI	MRI-ESM2-0	ssp585	Yukimoto, S., Koshiro, T., Kawai, H., Oshima, N., Yoshida, K., Urakawa, S., Tsujino, H., Deushi, M., Tanaka, T., Hosaka, M., Yoshimura, H., Shindo, E., Mizuta, R., Ishii, M., Obata, A., Adachi, Y. (2019). MRI MRI-ESM2-0 model output prepared for CMIP6 ScenarioMIP ssp585. v20191108. Earth System Grid Federation. https://doi.org/10.22033/ESGF/CMIP6.6929
NCC	NorESM2-MM	historical	Bentsen, M., OliviÃ¨, D.J.L., Seland, Ã˜., Toniazzo, T., Gjermundsen, A., Graff, L.S., Debernard, J.B., Gupta, A.K., He, Y., KirkevÃ¥g, A., Schwinger, J., Tjiputra, J., Aas, K.S., Bethke, I., Fan, Y., Griesfeller, J., Grini, A., Guo, C., Ilicak, M., Karset, I.H.H., Landgren, O.A., Liakka, J., Moseid, K.O., Nummelin, A., Spensberger, C., Tang, H., Zhang, Z., Heinze, C., Iversen, T., Schulz, M. (2019). NCC NorESM2-MM model output prepared for CMIP6 CMIP historical. v20191108. Earth System Grid Federation. https://doi.org/10.22033/ESGF/CMIP6.8040
NCC	NorESM2-MM	ssp126	Bentsen, M., OliviÃ¨, D.J.L., Seland, Ã˜., Toniazzo, T., Gjermundsen, A., Graff, L.S., Debernard, J.B., Gupta, A.K., He, Y., KirkevÃ¥g, A., Schwinger, J., Tjiputra, J., Aas, K.S., Bethke, I., Fan, Y., Griesfeller, J., Grini, A., Guo, C., Ilicak, M., Karset, I.H.H., Landgren, O.A., Liakka, J., Moseid, K.O., Nummelin, A., Spensberger, C., Tang, H., Zhang, Z., Heinze, C., Iversen, T., Schulz, M. (2019). NCC NorESM2-MM model output prepared for CMIP6 ScenarioMIP ssp126. v20191108. Earth System Grid Federation. https://doi.org/10.22033/ESGF/CMIP6.8250
NCC	NorESM2-MM	ssp370	Bentsen, M., OliviÃ¨, D.J.L., Seland, Ã˜., Toniazzo, T., Gjermundsen, A., Graff, L.S., Debernard, J.B., Gupta, A.K., He, Y., KirkevÃ¥g, A., Schwinger, J., Tjiputra, J., Aas, K.S., Bethke, I., Fan, Y., Griesfeller, J., Grini, A., Guo, C., Ilicak, M., Karset, I.H.H., Landgren, O.A., Liakka, J., Moseid, K.O., Nummelin, A., Spensberger, C., Tang, H., Zhang, Z., Heinze, C., Iversen, T., Schulz, M. (2019). NCC NorESM2-MM model output prepared for CMIP6 ScenarioMIP ssp370. v20191108. Earth System Grid Federation. https://doi.org/10.22033/ESGF/CMIP6.8270

NOAA-GFDL	GFDL-CM4	historical	Guo, H., John, J.G., Blanton, C., McHugh, C., Nikonov, S., Radhakrishnan, A., Rand, K., Zadeh, N.T., Balaji, V., Durachta, J., Dupuis, C., Menzel, R., Robinson, T., Underwood, S., Vahlenkamp, H., Bushuk, M., Dunne, K.A., Dussin, R., Gauthier, P.P.G., Ginoux, P., Griffies, S.M., Hallberg, R., Harrison, M., Hurlin, W., Malyshev, S., Naik, V., Paulot, F., Paynter, D.J., Ploshay, J., Reichl, B.G., Schwarzkopf, D.M., Seman, C.J., Shao, A., Silvers, L., Wyman, B., Yan, X., Zeng, Y., Adcroft, A., Dunne, J.P., Held, I.M., Krasting, J.P., Horowitz, L.W., Milly, P.C.D., Shevliakova, E., Winton, M., Zhao, M., Zhang, R. (2018). NOAA-GFDL GFDL-CM4 model output prepared for CMIP6 CMIP historical. v20180701. Earth System Grid Federation. https://doi.org/10.22033/ESGF/CMIP6.8594
NOAA-GFDL	GFDL-CM4	ssp245	Guo, H., John, J.G., Blanton, C., McHugh, C., Nikonov, S., Radhakrishnan, A., Zadeh, N.T., Balaji, V., Durachta, J., Dupuis, C., Menzel, R., Robinson, T., Underwood, S., Vahlenkamp, H., Dunne, K.A., Gauthier, P.P.G., Ginoux, P., Griffies, S.M., Hallberg, R., Harrison, M., Hurlin, W., Lin, P., Malyshev, S., Naik, V., Paulot, F., Paynter, D.J., Ploshay, J., Schwarzkopf, D.M., Seman, C.J., Shao, A., Silvers, L., Wyman, B., Yan, X., Zeng, Y., Adcroft, A., Dunne, J.P., Held, I.M., Krasting, J.P., Horowitz, L.W., Milly, C., Shevliakova, E., Winton, M., Zhao, M., Zhang, R. (2018). NOAA-GFDL GFDL-CM4 model output prepared for CMIP6 ScenarioMIP ssp245. v20180701. Earth System Grid Federation. https://doi.org/10.22033/ESGF/CMIP6.9263
NOAA-GFDL	GFDL-CM4	ssp585	Guo, H., John, J.G., Blanton, C., McHugh, C., Nikonov, S., Radhakrishnan, A., Zadeh, N.T., Balaji, V., Durachta, J., Dupuis, C., Menzel, R., Robinson, T., Underwood, S., Vahlenkamp, H., Dunne, K.A., Gauthier, P.P.G., Ginoux, P., Griffies, S.M., Hallberg, R., Harrison, M., Hurlin, W., Lin, P., Malyshev, S., Naik, V., Paulot, F., Paynter, D.J., Ploshay, J., Schwarzkopf, D.M., Seman, C.J., Shao, A., Silvers, L., Wyman, B., Yan, X., Zeng, Y., Adcroft, A., Dunne, J.P., Held, I.M., Krasting, J.P., Horowitz, L.W., Milly, C., Shevliakova, E., Winton, M., Zhao, M., Zhang, R. (2018). NOAA-GFDL GFDL-CM4 model output prepared for CMIP6 ScenarioMIP ssp585. v20180701. Earth System Grid Federation. https://doi.org/10.22033/ESGF/CMIP6.9268